This is a repository copy of *How old are the Mojave topographic dunes? The implications of new luminescence dating analyses from the Cady Mountains, Mojave Desert, southwest USA*.

White Rose Research Online URL for this paper:
https://eprints.whiterose.ac.uk/216040/

Version: Published Version
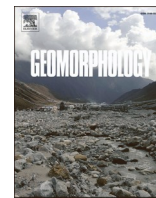
How old are the Mojave topographic dunes? The implications of new luminescence dating analyses from the Cady Mountains, Mojave Desert, southwest USA

Andrew S. Carr [a,*], Alex S. Hay [a], Mark D. Bateman [b], Ian Livingstone [c], D. Mark Powell [a]

[a] *School of Geography, Geology and the Environment, University of Leicester, University Road, Leicester LE1 7RH, UK*
[b] *Department of Geography, University of Sheffield, Winter Street, Sheffield S10 2TN, UK*
[c] *The Graduate School, University of Northampton, Northampton NN1 5PH, UK*

A R T I C L E   I N F O

A B S T R A C T

The aeolian landforms of the Mojave Desert in the SW USA have been studied in detail over the last three decades, particularly in terms of their relationship to the region's topography and Pleistocene climate / sediment supply histories, as well as wider developments, such as the aeolian "sediment state" concept. In this context, the evolution of the Mojave River and its associated palaeolakes is thought to have been a key control on long-term sediment supply to aeolian systems, and luminescence dating chronologies for a range of (resulting) aeolian landforms have been related to these hydrological changes. Here we argue that at least some of these aeolian chronologies need to be re-assessed.

We focus on luminescence chronologies for aeolian landforms within and marginal to the Cady Mountains, a mountain block adjacent to the Mojave River and palaeolake Manix, east of Barstow, California. We demonstrate that quartz in this locale exhibits several malign luminescence properties, and that low temperature K-feldspar infrared stimulated luminescence (IRSL) consistently exhibits high anomalous fading rates. Both contribute to age underestimation. We address these issues via post-infrared IRSL (pIRIR) and post-isothermal post-IR (pIt-IR) analyses of K-feldspars. The resulting ages span the last ~120 ka and imply phases of aeolian activity of a substantially greater antiquity than previously inferred. Notably, at one well-studied site – the Soldier Mountain sand ramp – the new ages suggest a landform dating not to Marine Isotope Stage (MIS) 1 or 2, as previously suggested, but more likely to MIS 5. The Cady Mountain record indicates that the only period of the last glacial cycle lacking evidence for aeolian sedimentation is ~40–9 ka, broadly consistent with expectations of increased regional humidity. These results also suggest that site topographic context may influence the age structure of aeolian deposits. In this instance, sand ramps consistently represent the oldest type of deposit (range ~ 40–120 ka), while early-mid Holocene dune accumulation is associated with sandsheets and valley-fill sands. Based on these findings, we argue that there is a need to critically re-assess the existing regional luminescence age database, and that there is potential to significantly revise our understanding of the region's aeolian system responses, and associated paleoenvironmental interpretations.

1. Introduction and context

The Mojave Desert of the southwest USA – characterised today by ephemeral rivers and rare inundation of lake basins (Enzel, 1992; Enzel and Wells, 1997) – experienced significant changes in hydrological balance throughout the Pleistocene, largely in response to the varying delivery of moisture from the Pacific Ocean (Enzel et al., 2003; Reheis et al., 2012; Wendt et al., 2018). At times these changes were sufficient to sustain perennial river flow, emergent groundwater and several palaeo-lakes (Meek, 1989, 1999; Enzel et al., 2003; Pigati et al., 2011; Reheis et al., 2014; Garcia et al., 2014; Miller et al., 2019). The aeolian dunes of the Mojave, and in particular the timing(s) of their formation in relation to regional hydrological change, have formed the basis of numerous discussions concerning long-term aeolian sediment system dynamics and have been used to inform our wider understandings of process-domain interactions (inter alia: Clarke and Rendell, 1998;

Kocurek and Lancaster, 1999; Tchakerian and Lancaster, 2002; Sweeney et al., 2020). Here, palaeohydrology in particular is invoked as playing an integral role in controlling sediment supply and availability to downwind dunes (Kocurek and Lancaster, 1999). An obvious way to test such hypotheses is to build chronologies that allow comparisons between records of aeolian sedimentation and palaeohydrological change (Clarke and Rendell, 1998; Tchakerian and Lancaster, 2002; Sweeney et al., 2020). This paper considers how to best develop the necessary chronologies of dune accumulation, and the reliability of existing chronological data in this region.

Topography is thought to have played an additional role in shaping the regional aeolian record via the presence of several topographically-controlled sand transport corridors (Zimbleman et al., 1995); here aeolian sediment is conceived as moving from sources to specific sinks via pathways mediated by the macro-scale basin and range topography (Evans, 1962; Smith, 1984; Clarke and Rendell, 1998; Muhs et al., 2003). The termini of transport corridors may be characterised by the presence of (free) dunefields, such as the Kelso dunes (Sharp, 1966; Fig. 1), but topographic dunes (per Livingstone and Warren, 2019) also occur adjacent to and at the termini of transport corridors. These manifest as climbing dunes and falling dunes and are often accompanied by sand ramps (Evans, 1962). Many sand ramps are seemingly relict, and as landforms characterised by interbedded aeolian sands, fluvial gravels and slope-derived talus, they have been interpreted as providing insights into long-term environmental change (Lancaster and Tchakerian, 1996; Tchakerian and Lancaster, 2002). Indeed, after their initial identification in the Mojave, sand ramps have been studied globally, often from a palaeoenvironmental perspective (e.g., Thomas et al., 1997; Bertram, 2003; Kumar et al., 2017; Rowell et al., 2018a, b; Schaetzl et al., 2018; Paichoon, 2020).

In terms of the timings of these landscape processes, there is a relatively long-history of luminescence dating within the Mojave, with several notable datasets developed for aeolian, lacustrine, and alluvial

fan deposits during the 1990s (Edwards, 1993; Clarke, 1994; Rendell et al., 1994; Wintle et al., 1994; Clarke et al., 1995, 1996; Rendell and Sheffer, 1996). These works employed a variety of multi-aliquot infrared stimulated luminescence (IRSL) and thermoluminescence (TL) methods applied to quartz and K-feldspar, as well as a single aliquot additive dose (SAAD) IRSL protocol applied to K-feldspars. Subsequently, optically stimulated luminescence (OSL) applied to single aliquots of quartz has been employed (Owen et al., 2007; Mahan et al., 2007; Bateman et al., 2012; Fuchs et al., 2015; Cyr et al., 2015; Sweeney et al., 2020). One of the largest luminescence datasets was produced for sand ramps by Rendell and Sheffer (1996). They used quartz / feldspar TL and feldspar IRSL on 78 samples from nine sand ramps, with the resulting ages interpreted as indicating phases of ramp accretion 30–20 ka, 15–7 ka and during the Late Holocene (Fig. 2). Ages seemingly coeval with (palaeo) Lake Mojave high-stands (Clarke and Rendell, 1998) were inferred to imply a need for frequent river flows to supply sediment to these landforms. Overall, sand ramp formation in this region has been interpreted as episodic, and to have peaked in the Late Pleistocene / Early Holocene (Tchakerian and Lancaster, 2002; Bateman et al., 2012; Fig. 2).

The Mojave chronological dataset is not, however, without inconsistencies. For example, Rendell and Sheffer's (1996) most intensively sampled sand ramp, Soldier Mountain, reveals stratigraphic age reversals and age differences between methods and minerals. A subset of K-feldspar IRSL ages, spanning 11–22 ka (rather than the less bleachable quartz TL signal) was later emphasised (Clarke and Rendell, 1998). From the same Solider Mountain sections, Bateman et al. (2012) produced a chronology using a single aliquot regeneration (SAR) protocol (Murray and Wintle, 2000) applied to multi-grain aliquots of quartz. The ages ranged between 11.6 ± 0.8 ka and 8.3 ± 0.8 ka, with the uppermost ages relatively close to those of Rendell and Sheffer (1996). However, samples from the lower section were markedly younger, implying a young, rapidly formed sand ramp. The authors noted this was
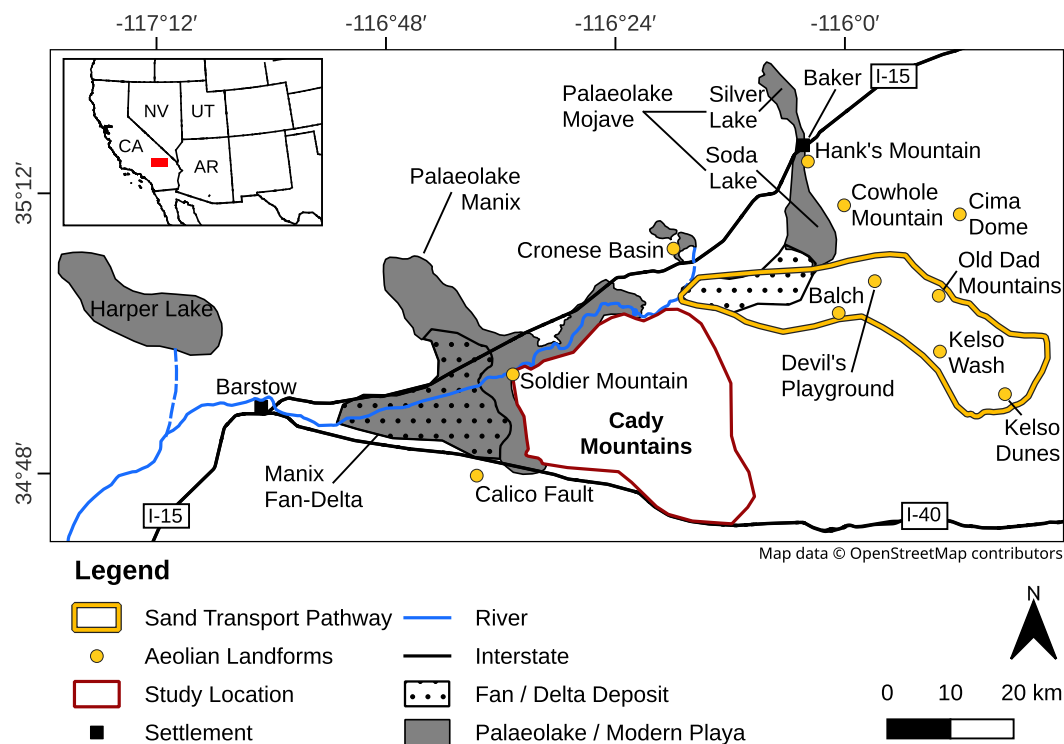
Fig. 1. Map of the study region, illustrating the course of the Mojave River, the position of the Cady Mountain block (the western-most limit is referred to as the western flank in Hay et al. (2021)) and the former extent of palaeo-Lakes Manix, Harper and Mojave (the latter comprising modern day Silver Lake and Soda Lake). The fan/delta deposits represent potential aeolian sediment stores (sources) for the Cady Mountains and the Kelso Dunes sand transport corridor (which is delineated in yellow). The locations of several previously published sites referred to in the text are shown, including several sand ramps (i.e. Hank's Mountain, Balch, Old Dad Mountains) sampled for IRSL dating by Rendell and Sheffer (1996).
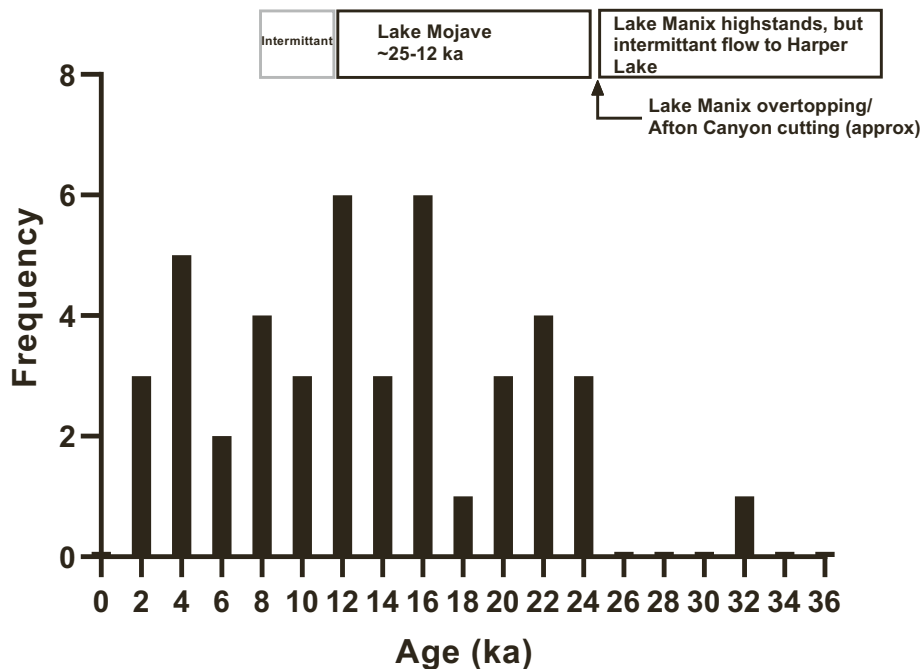
Fig. 2. Compiled luminescence (IRSL) ages from nine sand ramps in the Mojave (Rendell and Sheffer, 1996). Ages are plotted in 2 ka bins. These ages are shown in relation to: 1) the timing of the Lake Manix drainage (~25 ka) and 2) the occurrence of permanent (then intermittent) water in Lake Mojave (modern Soda and Silver Lake playas; Kirby et al., 2015; Honke et al., 2019). Coeval sand ramp formation and playa inundation were inferred to indicate the importance of hydrologically-mediated sediment supply as a control on sand ramp formation (Clarke and Rendell, 1998).

very difficult to reconcile with other geomorphic evidence at the site, notably the rate at which the clastic (i.e. slope) component could have been incorporated into the sand ramp. An obvious explanation for these discrepancies is that one or both of these chronologies is inaccurate.

The development of the single aliquot regeneration protocol (SAR; Murray and Wintle, 2000, 2003) resulted, in many contexts, in marked improvements in the accuracy and precision of luminescence chronologies (e.g. Murray and Olley, 2002; Rhodes, 2011). Recent work reviewing the use of published or "legacy" OSL age datasets has considered this a critical quality control factor (Small et al., 2017). The need for (small) single aliquot or single grain analyses, particularly as a means to evaluate the risk of incomplete bleaching was also highlighted as a key criterion (ibid). These factors alone present challenges for the (re)use / (re)interpretation of existing chronologies in the Mojave. Indeed, it is worth noting that even the more recent quartz SAR results present by Bateman et al. (2012) were based on large (9 mm 125–250 µm) aliquots averaging signals from several thousand grains; despite this, outlier aliquots were identified in their analyses.

Three specific dating challenges are likely pertinent to the Mojave sand ramps and associated topographic dunes: partial bleaching of the luminescence signal prior to burial, anomalous fading of K-feldspars and the variable luminescence characteristics of Mojave Desert quartz. In terms of incomplete bleaching, given the mixed aeolian and slope (talus) composition of many sand ramps, and the short transport distances from bedrock sources on the upper mountain front slopes, there is a risk that incompletely bleached grains are mixed with the aeolian sand component (Rendell et al., 1994).

A well-established limitation for IRSL dating of K-feldspars is the occurrence of anomalous fading, particularly for low stimulation temperatures (<100 °C; Wintle, 1973). The IRSL ages shown in Fig. 2 were all obtained using 50 °C IRSL measurements. Subsequently methods have been developed to correct for fading by quantifying a sample's fading rate (quantified as the "g-value"; Aitken, 1985; Auclair et al., 2003) and recent studies have shown that K-feldspar fading rates in the Mojave are quite high, reaching 6–11 % per decade for the 50 °C IRSL signal (Garcia et al., 2014; Carr et al., 2019; cf. Huntley and Lian, 2006,

their Fig. 2a). For this reason, it is likely (albeit not often stated) that many existing IRSL ages, such as those shown in Fig. 2, are age underestimates.

The development of post-IR IRSL (pIRIR) protocols for K-feldspars (Buylaert et al., 2009; Buylaert et al., 2012; see also Li et al., 2014; Zhang and Li, 2020) has the potential to mitigate the fading problem. The post-IR approach typically utilises a low temperature (often 50 °C) IRSL measurement to empty the most fading-prone electron traps, followed by a higher temperature ("post-IR"; often 225 or 290 °C) stimulation that detects a less fading-prone signal. Within the present study region Carr et al. (2019) tested several variants of the post-IR IRSL approach at Harper and Silver Lakes, and demonstrated significantly better agreement with independent dating for pIRIR measured at 225 °C and 290 °C (henceforth $pIRIR_{225}$ and $pIRIR_{290}$). The wider suitability of this approach across the region's topographic dunes and sand ramps is yet to be demonstrated, though recent work has produced promising results (Lancaster et al., 2022).

Finally, based on previous studies, Mojave quartz samples (unlike feldspar) have been observed to exhibit several problematic phenomena; viz low sensitivity, excessive thermal transfer, a weak or absent fast component (or non-trivial medium component) and the presence of feldspar inclusions (Lawson et al., 2012; Roder et al., 2012; Fuchs et al., 2015; Carr et al., 2019). Quartz OSL ages from sites with independent dating (the aforementioned Harper Lake and Silver Lake) have each twice (and independently) been shown to be substantial underestimates (Owen et al., 2007; Garcia et al., 2014; Carr et al., 2019). By contrast, some studies have reported quartz ages in agreement with other methods (Mahan et al., 2007; Cyr et al., 2015). It thus seems prudent to consider quartz OSL performance on a site-by-site basis and, where possible, with independent age control.

In summary, while there is a long history of applying luminescence methods to aeolian landforms within and downwind of the Mojave River catchment, the available data often reveal inconsistencies within sites and between methods. This probably reflects some combination of the issues outlined above. Elsewhere the re-application of modern single aliquot luminescence methods has led to significant re-evaluations of

some site chronologies (e.g. Duller and Augustinus, 2006; Rowell et al., 2018b) and given the foregoing, we propose that the ages of at least some Mojave aeolian deposits and sand ramps remain weakly constrained (and by corollary, as is their palaeoenvironmental significance). The aims of this paper are thus twofold: firstly, to test whether previous chronologies are indeed erroneous and to understand why. To achieve this, building on initial work on nearby sites with independent dating (Carr et al., 2019) we focus on comparisons between quartz OSL, low temperature IRSL and pIRIR methods. Secondly, through the wider application of the pIRIR approach we seek to establish a new chronology for a suite of sand ramps (including Soldier Mountain) and aeolian dunes. We consider sample behaviour, apparent ages for different methods and stimulation temperatures, the stratigraphic / internal consistency of these ages, and their potential environmental significance. We then review the wider implications for Quaternary dating within the Mojave Desert region.

2. Study area

In the context of a broader examination of the preservation of, and controls upon, topographically-controlled aeolian sediment accumulation within the Mojave (Hay et al., 2021), we obtained a suite of luminescence samples from the Cady Mountains, a mountain block ~50 km east of Barstow and immediately south of the contemporary Mojave River (Figs. 1 and 3). Today the climate is semi-arid, with mean annual precipitation ≤150 mm a^{-1} and annual potential evapotranspiration approximately 2000 mm a^{-1} (Blaney, 1957). Precipitation is primarily produced by cool season frontal systems, albeit with some contributions from summer convective systems. At various stages in the Middle and Late Pleistocene, under more humid conditions, the terminus of Mojave River lay adjacent to the Cady Mountains as (palaeo) Lake Manix (Meek, 1989, 2004; Reheis et al., 2012; Reheis and Redwine, 2008; Reheis et al., 2021). Lake Manix comprised several sub-basins, with the southern (Troy Basin) and central (Cady Basin) basins abutting the Cady Mountains, and the Coyote Basin located north of the modern Mojave River channel (Fig. 3). Lake Manix achieved several high stands at or close to 543 m above sea-level during marine isotope stages 3 and 2 (Reheis et al., 2015). At ~25 ka overtopping in the downstream Afton Canyon resulted in a breach and ultimately, drainage of the lake, connecting the Mojave River to Lake Mojave (Kirby et al., 2015; Honke et al., 2019), which persisted until ~12 ka (now represented by Soda and Silver Lake playas; Fig. 1).

The western Cady Mountains are mantled by an extensive, but variably thick cover of aeolian sands (Fig. 3). The distribution of this sand, along with evidence from ventifacts (Laity, 1992; Hay et al., 2021), implies a sediment source largely to the west – putatively the Manix fan delta (Fig. 3) or Mojave River (Laity, 1992). Although land-cover mapping of the Cady Mountains indicates widespread surficial aeolian sand cover, morphometric analysis has shown that >90 % of mapped aeolian sands actually occur in four meso-scale topographic contexts or
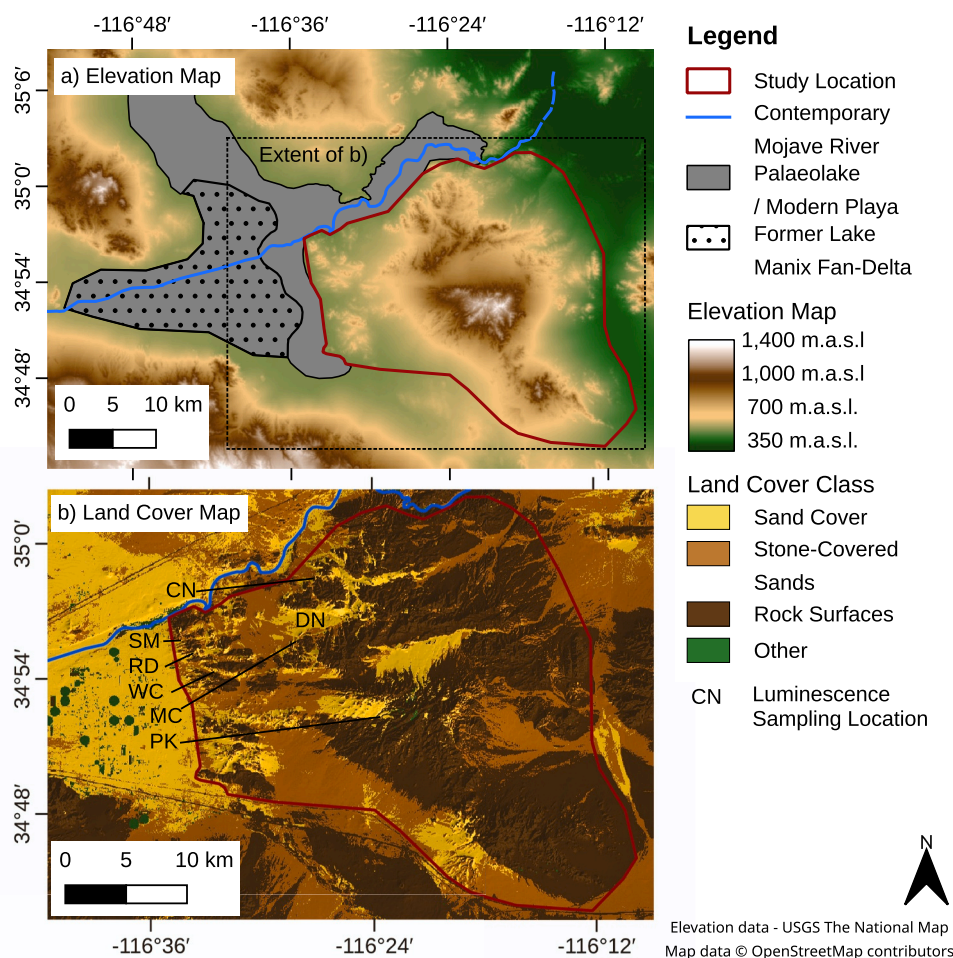
Fig. 3. A) Map of the sampling area showing the topography of the Cady Mountains in relation to the modern Mojave River, Lake Manix and the Manix fan delta (the proposed aeolian sediment source); B) shows the distribution of land cover classes within and adjacent to the Cady Mountains overlain on a DEM hill-shade (Hay et al., 2021). Here, the Sand Cover and Stone-Covered Sand classes represent largely aeolian sediments of varied thickness, with the latter characterised by desert pavements of varying degrees of development. The locations of the sample sites in this study are indicated (SM = Soldier Mountain; RD = Royalty Drive; WC=Western Cady; MC = Middle Cady; PK=Cady Peak; DN=Cady sandsheet; CN=Cady North).

"accommodation space types" (Hay et al., 2021). These are classed as Slopes, Plains, Valley-Fills, and a "Slope-Valley composite" type (Figs. 4 and 5). Specific landforms within these accommodation spaces comprise climbing / falling dunes and sand ramps (on Slopes), sand-sheets (on Plains) and "valley fill dunes" (Ellwein et al., 2011) within valleys orientated broadly parallel to the prevailing winds. In areas of high sediment supply, notably along the northern mountain block flank adjacent to the Mojave River, the pre-existing topography has been sufficiently buried to produce a composite Slope-Valley (fill) type. Here the lower mountain front Slopes (i.e. piedmont surface) and the valleys emerging from the mountain block are connected via a near continuous mantle of interbedded aeolian sands, and coarse-grained (channel and slope) sediment, with the latter more dominant in mountain-proximal locations. Hay et al. (2021) hypothesised that the topographic/geomorphic contexts of each of these accommodation space types will impart variability in both the rates and timings of sediment accumulation and sediment preservation potential. This was a key motivation for sampling these deposits for luminescence dating.

2.1. Sample sites

Sampling was conducted in reference to the aeolian sediment accommodation space types identified in Hay et al. (2021). We sampled the Soldier Mountain quarry exposures used by Rendell and Sheffer (1996), Lancaster and Tchakerian (1996) and Bateman et al. (2012), obtaining samples from the upper, middle and base of the exposures, mapping to Bateman et al.'s (2012) units III, IV and V (respectively, SM13-2-1, SM13-3-1 and SM13-1-1; Fig. S1a). Also sampled was a sand ramp on the western flank of the Cady Mountains (Royalty Drive (RD14-1-1 and RD14-1-2 Fig. S1b) and two sand ramps in the interior of the mountain block; Middle Cady (MC13-1-1 and MC13-1-2 Fig. S1c) and Cady Peak (PK14-1-1 through PK14-1-4 Fig. S1d). The latter are less well exposed, and are associated with more distant and less substantial flanking rock-slopes.

The Western Cady site (WC14-1-1 through WC14-1-3) targeted a Valley-fill sand, which comprised a 3.5 m exposure of aeolian sands close to the top of an E-W orientated valley on the western flank of the Cady Mountains (Figs. 3 and 4, Fig. S1e; see Hay et al., 2021 their Fig. S4). The most extensive example of the sandsheet type was the ~18 km^2 site DN, located with the north central mountain block (Fig. 4) downwind of the Soldier Mountain/Royalty Drive sand ramps. Its lithology was however more variable than the homogenous sandy upper surface implied; while the uppermost unit comprised, moderately sorted fine-medium grained sands, at depth several discontinuous stone layers with gravel clasts and granule lenses were apparent (Fig. S1f).

Along the northern margins of the Cady Mountains sand cover associated with the Valley-Fill class merges into a partially incised piedmont slope unit (Fig. 4) forming an example of Hay et al.'s (2021) Slope-Valley composite. The slope element comprised a low-angle concave surface incised by several channels, which at one locale (henceforth Cady North – CN; Fig. S1g) provided access to an 8 m section. This revealed a sequence of inter-bedded sands and gravel-boulder units separated by a distinct, laterally-extensive palaeosol (Fig. 5). This soil, which was observed outcropping at approximately the same altitude at distances of up to 1 km from the sample site, is in its upper parts rubified, with clear loss of pre-existing bedding structure and abundant preserved rootlets. Carbonate nodules, in places coalescing to more massive carbonates, are found immediately below the most rubified layers (Fig. 5b). Upslope, the flanks of the contiguous valley-fill section of this composite form were generally poorly exposed. However, it was possible to sample aeolian sands within a feeder valley (sample CN-Valley) 1.6 km upstream (southeast) of the channel position sampled at CN.

3. Methods

Sites were sampled following manual excavation or cleaning of natural sedimentary sections with sections logged in the field using standard methods. All luminescence samples were collected using steel tubes.

3.1. Sample preparation

Sample preparation was conducted in the luminescence laboratory at the University of Leicester, UK. The ends of each sample tube were removed and used to estimate sample water contents and external beta dose rates. Samples were treated with HCl and H_2O_2 to remove carbonates and organic matter (respectively). They were then wet sieved to 180–212 μm, with density separations performed using LST Fastfloat at 2.7 g cm^{-3} (to remove heavy minerals) and 2.58 g cm^{-3} to separate the quartz-rich and potassium feldspar-rich fractions. The quartz fractions were etched in concentrated (48 %) HF for 45 min and the feldspar fractions were etched in 10 % HF for 10 min to remove the outer alpha-irradiated portion of the grain and/or grain coatings.

3.2. Luminescence measurements

All OSL and IRSL measurements (Table S1) were performed on 2 mm aliquots comprising ~100–150 grains in a Risø DA20 TL/OSL reader. For quartz, stimulation (60 s at 125 °C) was provided by blue LEDs (wavelength 470 nm) with the resulting OSL detected via a U-340 detection filter. Where applied, a single aliquot regeneration protocol was used (Murray and Wintle, 2000, 2003), with 240 °C (for 10 s) and 220 °C (cut heat) preheats utilised for the natural/regenerated and test dose measurements (respectively). Saturating exponential dose-response curves were fitted to the data and equivalent doses (D_e) and their uncertainties were estimated using the Monte-Carlo simulation with the *Analyst* (v4.57) software (e.g. Duller, 2007). For K-feldspar, IR stimulation was by IR diodes (wavelength 870 nm), with detection of the resulting (blue-violet) IRSL through a combination of Schott BG39 filters and Corning 7–59 filters (detection range 320–450 nm). The post-IR IRSL single aliquot regeneration protocols comprised a low temperature IRSL measurement at 50 °C, followed by IRSL measurements at either 225 °C (pIRIR$_{225}$) or 290 °C (pIRIR$_{290}$). Stimulation was for 100 s (50 °C IR) and then for a further 100 s at 225/290 °C (post-IR). Preheat temperatures (Fig. S3) were 250 °C / 320 °C for 60 s for the pIRIR$_{225}$ and pIRIR$_{290}$ measurements (respectively), with a 290/325 °C high temperature (60 s) bleach carried out after each SAR cycle (Buylaert et al., 2009; Buylaert et al., 2012). The test dose (T_n or T_x) was scaled to between one quarter and one third of the equivalent dose (Colarossi et al., 2018). Fading rate measurements followed Auclair et al. (2003) and g-values were determined using the *Luminescence* R package (Kreutzer, 2024; Kreutzer et al., 2024).

3.3. Environmental dose rates

Details of the dose rate determinations are presented in Table S6. The external gamma dose rates were obtained in-situ using an Ortec Na-I portable gamma spectrometer. The external beta dose rates were determined from the dried and milled sample tube ends using a Risø GM Beta counter (Bøtter-Jensen and Mejdahl, 1988; calculations following Jacobs and Roberts, 2015). Dose rates were corrected for grain size (Mejdahl, 1979), water content (Aitken, 1985) and HF etching (Bell, 1979). The internal K and Rb concentrations of 12.5 ± 0.5 % and 400 ± 100 ppm respectively were adopted from Huntley and Baril (1997) and Huntley and Hancock (2001). Cosmic dose rates, based on the measured sample depths were calculated using the *Luminescence* R package (Burow, 2024; Kreutzer et al., 2024) following Prescott and Hutton (1994) with a 10 % relative uncertainty included. Final dose rate uncertainties incorporate 3 % relative uncertainties for the grain size,
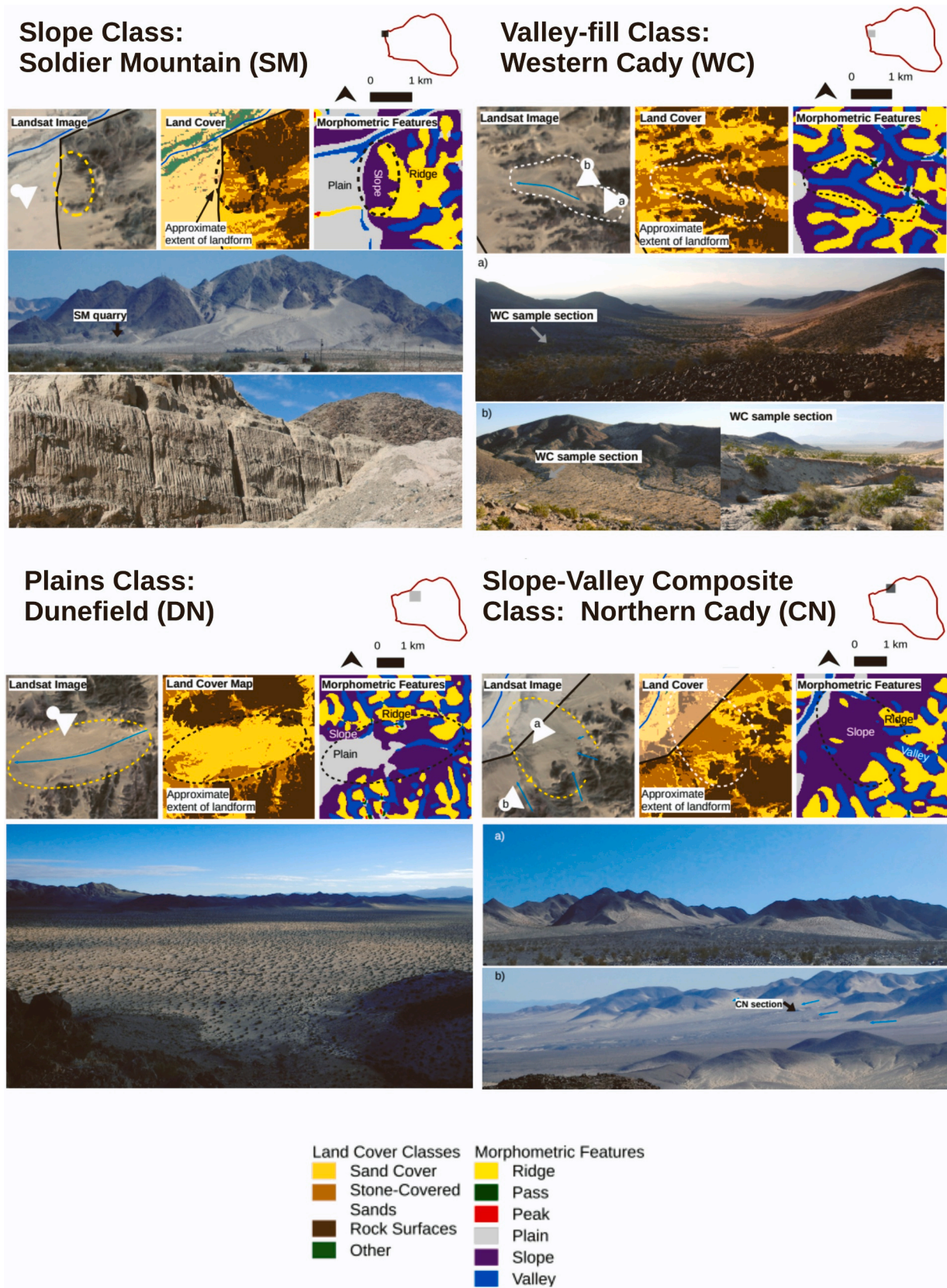
Fig. 4. Images of the four main aeolian sand accommodation space types identified by Hay et al. (2021). Red polygons with accompanying grey boxes show the location of each site within the Cady Mountains (as delineated in Fig. 3). In the Slope-Valley Composite class the piedmont slopes are mantled by a stratified mixture of aeolian sands and fluvial/colluvial gravels, akin to a sand ramp, but the aeolian sands extend beyond the piedmont junction and into the mountain block (e.g. panel A bottom right).
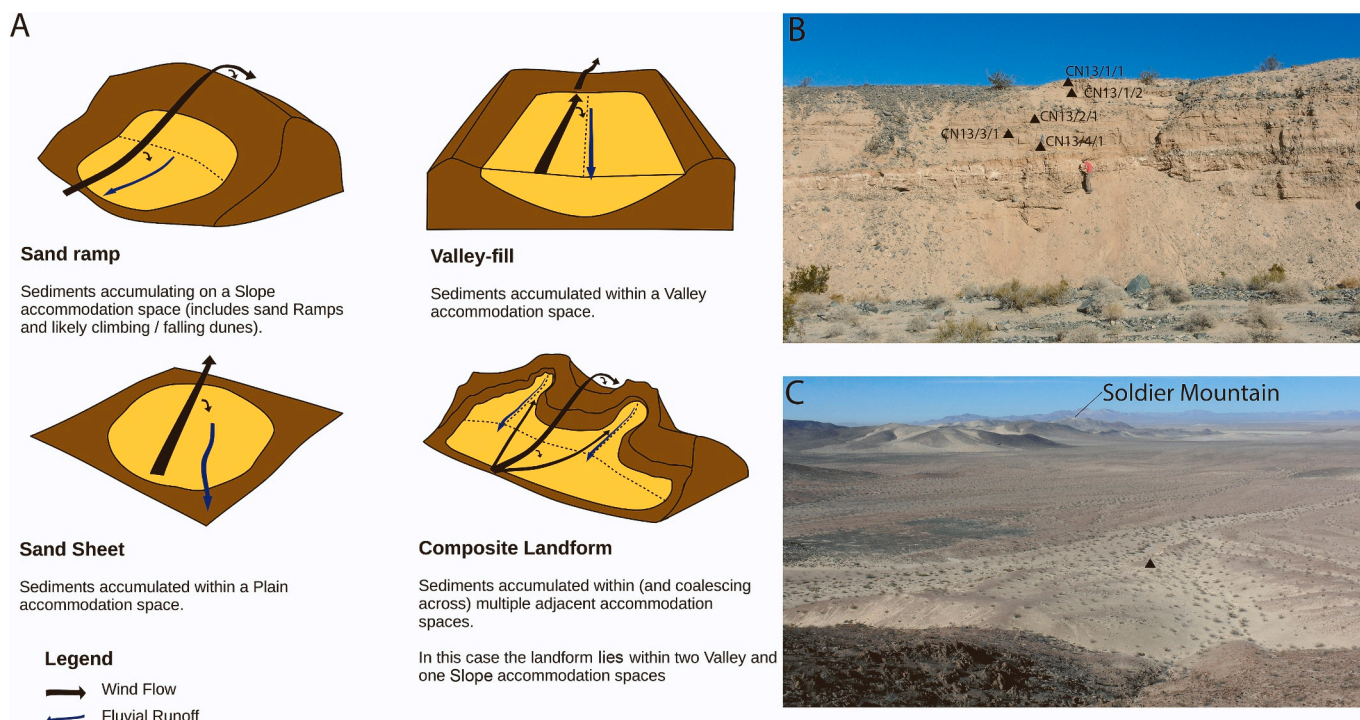
Fig. 5. A) Illustration of the four classes of accommodation space identified in Hay et al. (2021). B) view of the CN section (location shown in Fig. 3), showing the inter-bedded sands and gravels of the distal Slope-Valley Composite accommodation space type. The upper samples are labelled, with a palaeosol located mid-section close to the figure. The upper surface lies at 610 m above sea level. C) view from above the MC (Middle Cady) sand ramp looking northwest. The black triangle shows the approximate location of the sampled section. The sand ramp is partly incised with a darker coloured desert pavement developed on undissected surfaces. The leeward peak of Soldier Mountain is highlighted in the distance, with the southern margins of DN sandsheet located off to the extreme right of the photo.

water and HF etching attenuation factors. It was assumed that the as-measured water content was appropriate, with a 2 % (absolute content) uncertainty propagated into the final dose rate uncertainties.

4. Results

4.1. Quartz OSL properties and apparent ages

Preliminary measurements at Soldier Mountain utilised quartz OSL and were initially anticipated to replicate the results in Bateman et al. (2012). However, it was immediately apparent that these samples presented challenges. Despite routine density separation at 2.58 g cm^{-3} to remove K-feldspars, followed by HF etching and re-sieving, a consistently bright IRSL signal was observed, implying persistent feldspar contamination (Lawson et al., 2012). For the new (Leicester) Soldier Mountain samples, this IRSL signal was greatly reduced with a repeated 2.58 g cm^{-3} density separation, an additional short (15 min) HF etch, and prolonged HCl treatment to remove (often abundant) fluoride precipitates produced during HF etching.

To consider the quality and properties of these re-processed quartz extracts more systematically we applied the compositional test proposed by Lawson et al. (2012, 2015), which assesses thermal quenching and IR depletion to identify the most "quartz-like" and most "feldspar-like" behaviours. Thermal quenching (Spooner, 1994) relates to an observed reduction in quartz OSL intensity at higher stimulation temperatures (>150 °C), contrasting with a typically enhanced signal intensity seen for feldspars held at elevated temperatures. The results (Fig. 6) are shown in reference to known-age underestimating quartz from Silver Lake (SL) and Harper Lake (HL). The Cady Mountain quartz showed a range of behaviours within and between sites. Most samples plot in the upper right and have relatively high normalised-IR ratios (implying a dominantly quartz-like signal), and some exhibit quartz-like thermal quenching. However, despite relatively quartz-like IR ratios, several
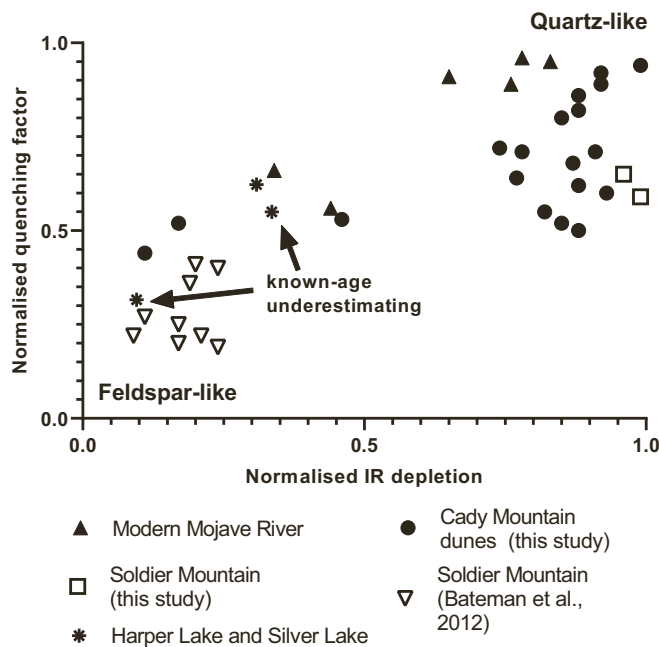
Fig. 6. Results of the quartz composition test (2 mm aliquots, following Lawson et al. (2012, 2015)). The age-underestimating Harper and Silver Lake samples (asterisks) are highlighted with the arrows. The Bateman et al. (2012) samples were obtained using the original quartz extracts from said paper. The quenching factor compares OSL signals obtained at 125 and 200 °C, while the IR depletion compares 125 °C OSL signals with and without a prior 40 s (50 °C) IR stimulation; the presence of K feldspar will induce a significant reduction in the latter signal. In each case the results are normalised to those obtained for pure quartz and K-feldspars (values of 1 and zero respectively).

samples (including Soldier Mountain) exhibited normalised thermal quenching ratios akin to those at Harper and Silver Lake. The data obtained for modern Mojave River sands – a likely Cady Mountain sediment source – also showed substantial variability. We also re-examined the original extracts used in Bateman et al. (2012) (plotted as inverted open triangles). The feldspar-like behaviour of these samples is quite apparent, and it seems that here routine quartz preparation methods and feldspar contamination identification measurements need to be carefully checked (Lawson et al., 2012). However, it is unlikely that these varied properties reflect only feldspar contamination. The (post-IR) quartz OSL decay curves (Leicester extracts) also varied significantly in their form. Tellingly, linear modulated OSL (LM-OSL) measurements indicated that even the most "quartz-like" samples, (per the composition test) exhibited a weak or absent quartz fast component, including Soldier Mountain (Fig. S2).

To provide a benchmark for the post-IR-IRSL methods that follow, and to evaluate apparent quartz "age" variability, equivalent doses were determined for a subset of quartz samples using a post-IR blue SAR protocol, with a 60 s 50 °C IR stimulation prior to each OSL measurement. Early background signal subtraction (Cunningham and Wallinga, 2010) was also used to maximise the contribution of the OSL fast component, and quartz fast ratios (Durcan and Duller, 2011) were estimated (Tables S1 and S2; Fig. S2). There was clear variability in fast ratio, and aliquot rejection rates (using standard recycling ratio and recuperation signal metrics) were high for several samples. Dose

recovery (Murray and Wintle, 2003) experiments indicated that pre-heating temperatures >220 °C were required for acceptable results (cf. Bateman et al., 2012). Although the mean dose recovery ratio was often within 10 % of unity, inter-aliquot scatter was elevated. Considering Soldier Mountain specifically, fast ratios were typically low (mean 6 ± 2 %, $n = 15$; Table S2), and when early background signal subtraction was employed three quarters of the otherwise acceptable aliquots were rejected due to saturation of the dose-response curve (Fig. S2; L_n/T_n greater than L_{max} and or infinite L_n/T_n uncertainties).

On face-value these initial OSL measurements imply that the DN sandsheet and the upper parts of the CN section are Holocene in age, and that the lower CN section and the PK sand ramp date to the late Pleistocene. However, the results imply a clear risk of age inaccuracy, likely due to combinations of K-feldspar contamination and a weak quartz fast component. Both feldspar contamination and non-trivial medium or slow component contributions may generate quartz age underestimations (Steffen et al., 2009). Given the apparent saturation of the quartz OSL signal, the Soldier Mountain sand ramp is possibly older than Rendell and Sheffer (1996) or Bateman et al. (2012) inferred (Table S2). Quartz saturation was not previously reported for this site; its identification (given the higher saturation dose of feldspars) may indicate better isolation of a quartz signal via the additional laboratory preparation steps and the early background subtraction approach.

Table 1

Single aliquot IRSL and pIRIR age summaries. Details of the equivalent dose measurements and the dose rate determinations are presented in tables S5 and S6. The pIRIR$_{225}$ ages have been fading corrected following Huntley and Lamothe (2001) using site-specific g-value$_{2days}$, implemented in the *Luminescence* R package (Kreutzer, 2024; Kreutzer et al., 2024). This excludes WC, where the all-site mean g-value$_{2days}$ was used. The IR50 ages were not routinely fading-corrected as this generated very large age uncertainties for several samples. Preliminary pIt-IR ages are each derived from the mean of 4 measured aliquots. Green shaded cells are preferred age estimates.

Sample	Depth (m)	Quartz dose rate	Quartz age (ka)	K-Feldspar dose rate	IR 50 (uncorrected) age (ka)	pIRIR$_{225}$ (uncorrected) age (ka)	pIRIR$_{225}$ fading corrected age (ka)	pIRIR$_{290}$ age (ka)	pIt-IR age (ka)
CN slope-valley composite									
CN13-1-1	0.4			4.78 ± 0.17	10 ± 1	21 ± 1	Nd	Nd	
CN13-1-2	0.8	3.63 ± 0.14	10 ± 1	4.47 ± 0.15	8 ± 1	16 ± 1	Nd	22 ± 2	
CN13-2-1	2.8			4.52 ± 0.14	13 ± 1	25 ± 2	Nd	28 ± 2	
CN13-3-1	3.8			4.48 ± 0.15	14 ± 1	26 ± 1	Nd	Nd	
CN13-4-1	4.6	3.51 ± 0.14	12 ± 1	4.36 ± 0.15	5.4 ± 0.3	10 ± 1		12 ± 1	
CN13-5-1	5.6			4.27 ± 0.15	27 ± 2	55 ± 3	72 ± 5	69 ± 4	83 ± 4
CN13-6-1	7.7			4.52 ± 0.15	24 ± 1	57 ± 3	75 ± 5	73 ± 4	
CN13-7-1	8.1	3.58 ± 0.15	36 ± 2	4.43 ± 0.16	26 ± 2	52 ± 3	68 ± 5	67 ± 3	
CN-Valley	0.5			4.91 ± 0.20	31 ± 2	66 ± 4	87 ± 7	95 ± 6	
Sand ramps									
SM13-1-1	2.0			4.29 ± 0.14	26 ± 1	53 ± 3	71 ± 7	67 ± 4	78 ± 5
SM13-3-1	5.0	3.62 ± 0.14	>45	4.34 ± 0.15	28 ± 1	55 ± 3	74 ± 7	78 ± 4	87 ± 5
SM13-2-1	14.5			4.48 ± 0.15	32 ± 2	74 ± 4	99 ± 9	Nd	
MC13-1-2	2.1			4.58 ± 0.14	35 ± 2	70 ± 4	92 ± 6	118 ± 8	
MC13-1-1	3.1			4.50 ± 0.15	38 ± 2	78 ± 4	83 ± 6	115 ± 6	
PK14-1-4	0.5			4.61 ± 0.15	16 ± 1	32 ± 2	39 ± 3	39 ± 2	
PK14-1-3	1.3			4.63 ± 0.15	17 ± 1	32 ± 2	39 ± 3	Nd	
PK14-1-2	1.6			4.76 ± 0.16	17 ± 1	32 ± 2	39 ± 3	Nd	
PK14-1-1	2.0	3.65 ± 0.13	42 ± 3	4.52 ± 0.15	16 ± 1	36 ± 2	44 ± 3	41 ± 2	
RD14-1-3	0.6			4.81 ± 0.17	0.7 ± 0.1	0.7 ± 0.1	Nd	Nd	
RD14-1-2	0.9			4.70 ± 0.16	26 ± 2	69 ± 3	90 ± 5	96 ± 6	
RD14-1-1	1.2			4.65 ± 0.16	25 ± 1	67 ± 3	92 ± 5	94 ± 6	
Sand sheet									
DN14-1-4	0.8			4.41 ± 0.14	3.6 ± 0.3	7.8 ± 0.7	Nd	Nd	
DN14-1-3	1.3			4.54 ± 0.15	7.3 ± 0.5	16 ± 1	Nd	19 ± 3	
DN14-1-2	1.8	3.67 ± 0.14	7.4 ± 1.2	4.51 ± 0.15	6.6 ± 0.6	15 ± 1	Nd	15 ± 2	
DN14-1-1	2.3	3.63 ± 0.14	5.5 ± 0.6	4.48 ± 0.15	2.9 ± 0.2	5.7 ± 0.4	6.6 ± 0.6	5.5 ± 0.4	
Valley-fill									
WC14-1-1	0.7			4.79 ± 0.16	2.1 ± 0.1	3.7 ± 0.2	4.3 ± 0.3	4.3 ± 0.3	
WC14-1-2	1.9			4.50 ± 0.15	2.3 ± 0.1	4.6 ± 0.2	5.3 ± 0.3	Nd	
WC14-1-3	3.5			4.41 ± 0.16	3.0 ± 0.2	5.3 ± 0.3	6.2 ± 0.3	6.5 ± 0.4	

4.2. pIRSL dating

To re-evaluate the chronology of Soldier Mountain, and to explore the ages of topographic dunes across the Cady Mountains more widely, we therefore developed a chronology using a post-IR IRSL approach. For both pIRIR$_{225}$ and pIRIR$_{290}$ SAR protocols, the samples produced bright IRSL signals, low levels of recuperation and excellent dose recovery across a range of doses and stimulation temperatures (Fig. S4, Table S3). We also confirmed the previous reports of high fading rates for low temperature IRSL measurements. These IR$_{50}$ g-values (mean 8.6 $\pm$ 0.8 %) were markedly reduced with a post-IR protocol (2.6 $\pm$ 0.2 % for pIRIR$_{225}$ and 1.7 $\pm$ 0.3 % for pIRIR$_{290}$; Table S4, Fig. S6).

The natural equivalent doses for multi-grain (2 mm) aliquot IR$_{50}$, pIRIR$_{225}$ and pIRIR$_{290}$ analyses are shown in Tables 1 and S5 and in Fig. 7. In all cases the ages were based on the central age model weighted mean (Galbraith et al., 1999). All sample D$_e$ distributions were overdispersed. In some instances, this reflected a small number of outlier aliquots (identified using nMAD; Normalised Median Absolute Deviation; e.g. Clarkson et al., 2017; Fig. S7), but some samples exhibited rather broad D$_e$ distributions. Overdispersion (OD) was often significantly higher for samples with equivalent doses <100 Gy, as might be anticipated if incomplete bleaching was a significant factor contributing to this OD (Fig. 7).

Considering Soldier Mountain, the pIRIR ages (pIRIR$_{225}$ 53–74 ka and pIRIR$_{290}$ 67–78 ka) are substantially older than those presented by Rendell and Sheffer (1996) and Bateman et al. (2012). They are however in stratigraphic order and in fact quite comparable to the results obtained from some of the other new sites, most notably the samples below the palaeosol at Cady North (CN: pIRIR$_{225}$ 52–57 ka and pIRIR$_{290}$ 67–73 ka). The ages for the Royalty Drive (RD) (RD: pIRIR$_{225}$ 67–69 ka and pIRIR$_{290}$ 94–96 ka) and Middle Cady sand ramps (MC, pIRIR$_{225}$ 70–78 ka; pIRIR$_{290}$ 115–118 ka) are older still, while the up-valley component at the CN slope-valley composite site is older than the slope/piedmont component (CN-Valley; pIRIR$_{225}$ 66 $\pm$ 4 ka and pIRIR$_{290}$ 95 $\pm$ 6 ka). Considering younger sites, at the Valley-fill site WC we observe stratigraphically concordant pIRIR$_{225}$ (3.7–5.3 ka) and pIRIR$_{290}$ (4.3–6.5 ka) ages. Two sites have problematic chronologies, with stratigraphically inverted ages observed in the upper section at CN (i.e. samples above the palaeosol; Fig. 4B) and age inversions in the DN sandsheet from the mountain block interior (Table 1; Fig. S1f).

The mean g-value$_{2days}$ for the pIRIR$_{225}$ signal is 2.6 $\pm$ 0.2 % per decade (Table S4), with the $n = 7$ measured g-values consistent with a common value (assessed per Galbraith, 2003). This is comparable to the values reported for Harper and Silver Lakes, where independent dating suggested fading correction of pIRIR$_{225}$ ages was necessary (Carr et al., 2019). The fading rate is further reduced for the pIRIR$_{290}$ signal, but comes with a greater risk of incomplete bleaching (e.g. Smedley et al., 2015). Indeed, given the aforementioned age inversions, the unexpectedly older ages obtained for Solider Mountain, and the expected

contribution of sediments from adjacent bedrock slopes, incomplete bleaching is perhaps the pre-eminent concern for the post-IR IRSL analyses.

One internal check for incomplete bleaching is to compare ages obtained from signals known to have different bleaching characteristics (Murray et al., 2012); the rationale being that it is very unlikely an incompletely bleached sample will produce the same ages for signals that bleach at significantly different rates. Such differences in bleaching rate have been unequivocally demonstrated for the IR50 and post-IR signals obtained from Mojave River K feldspar (McGuire and Rhodes, 2015; see also Fig. S5). Here we observe that for the Holocene valley fill sands site WC, fading correction brings both the IR50 and pIRIR$_{225}$ ages into excellent agreement with the harder to bleach pIRIR$_{290}$ ages (Table 1), implying adequate bleaching of all three signals. Such comparisons are more challenging for older samples, where fading correction of the IR50 signal generates large age uncertainties and is potentially inappropriate (Huntley and Lamothe, 2001). Notwithstanding, there is often reasonable agreement across the sites between the fading-corrected pIRIR$_{225}$ ages and the pIRIR$_{290}$ ages (Table 1). A further means to assess whether the age differences between IR50 and post-IR results reflect only the effects of fading is to plot the pIRIR$_{225}$ pIRIR$_{290}$ and IR50 data together (Fig. 8). Following Buylaert et al. (2013), samples plotting significantly below the fitted lines can be interpreted as having an incompletely bleached pIRIR$_{290}$ or pIRIR$_{290}$ signal (i.e. the pIRIR$_{225}$ or the pIRIR$_{290}$ D$_e$ is unusually large relative to the IR50 D$_e$). Given the measurement uncertainties, the results in Fig. 8 suggest only three samples (MC13-1-2 RD14-1-1 and DN14-1-3) exhibit differences that may reflect more than the effects of fading. The appearance of DN14-1-3 in both plots is not surprising given the aforementioned stratigraphic age inversions at the DN site (Table 1). The findings for MC13-1-1 are less expected given the otherwise stratigraphically concordant ages and low OD (though considering uncertainties it could still be considered to plot close to the fitted line). RD14-1-1 plots below the fitted line for the IR50-pIRIR$_{290}$ comparison (but not in the pIRIR$_{225}$ - pIRIR$_{290}$ comparison), and the significance of this is hard to evaluate given the resulting age is consistent with the sample stratigraphically above (RD14-1-1), which is within uncertainties of the fitted line (10 % range).

Finally, we evaluated the question of fading via the application of a post isothermal TL post-IR IRSL protocol to a small subset of samples (pIt-IR; Lamothe et al., 2020). In this method, rather than estimating the anomalous fading rate (g-value) with a sequence of delayed measurements (and potentially applying an age correction; e.g. Huntley and Lamothe, 2001), a set of isothermal TL (ITL) measurements of increasing duration is made prior to the IR50 and pIRIR$_{225}$ L$_x$ measurements that are used to construct the dose-response curves (Table S1). This serves to increase the measured IR50 and pIRIR$_{225}$ equivalent doses (as the L$_n$/T$_n$ measurements do not receive this ITL pre-treatment), and the ITL duration for which identical equivalent doses are obtained is inferred to
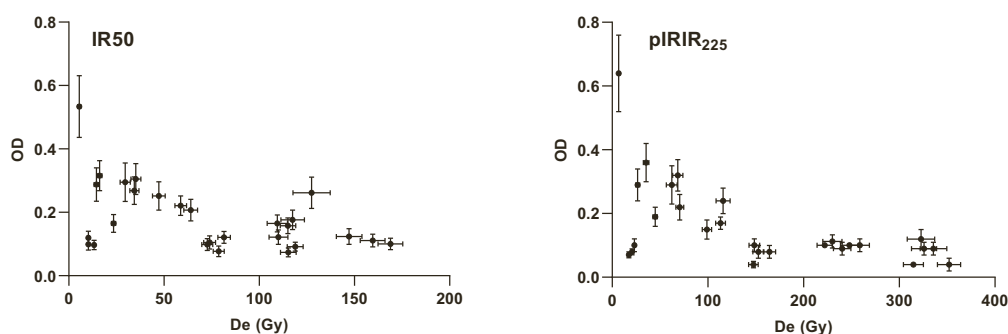

Fig. 7. Sample Central Age Model (CAM) equivalent dose (D$_e$) plotted relative to the associated overdispersion parameter. Data are for all accepted (2 mm) aliquots from all samples (no outlier removal). Note the three samples with low D$_e$/low OD on the lower left of each plot. These are from valley-fill site WC, where the ages are also in the correct stratigraphic order.
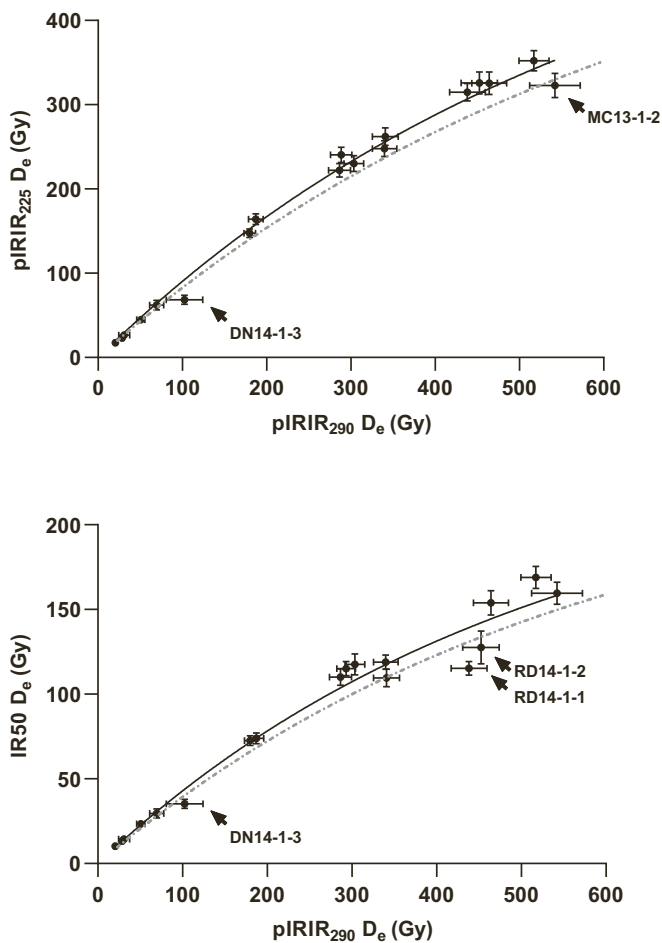
Fig. 8. Comparison (following Buylaert et al., 2013) of the single aliquot IR50 vs. pIRIR$_{290}$ and pIRIR$_{225}$ vs. pIRIR$_{290}$ CAM equivalent doses, fitted as y = a*(1-exp$^{(bx)}$). Grey fitted line = +10 %. Samples plotting below and to the right of the fitted or 10 % line are potentially incompletely bleached.

be indicative of the true radiation dose absorbed by the sample (ibid). We initially evaluated this protocol by applying it to two additional sites. The first was SL14–1 from the Silver Lake Quarry site (Carr et al., 2019) for which independent age control is available (Owen et al., 2007). The second sample (MJ22/14/2) was from the Lake Manix fan delta sediments exposed at the Harvard Road Mojave River crossing. This site, 5 km upwind (west) of Soldier Mountain, lies unambiguously within the sediment source zone for the Cady Mountains. Although it lacks independent numerical age control, it lies immediately west of the late Pleistocene limit of Lake Manix (Reheis et al., 2012) and has been exposed (and thus predates) by the post-Manix drainage incision of the Mojave River (Miller et al., 2019). We therefore expect ages close to or prior to the Marine Isotope Stage (MIS) 2 drainage of Lake Manix.

The pIt-IR results for both test samples conformed with age expectations (Table S7). The pIt-IR ages are (as expected) greater than the IR50 ages and the uncorrected pIRIR$_{225}$ ages. There is reasonable agreement, given uncertainties, between the pIt-IR ages and the fading-corrected pIRIR$_{225}$ or pIRIR$_{290}$ ages. For sample SL14-1 there is also good agreement with the existing radiocarbon dating (Table S7), suggesting the combination of preheating temperature and ITL temperature (270°C) is appropriate. Ages for three samples from the Cady Mountains (CN13-5-1, SM13-1-1 and SM13-3-1; Table 1) are in reasonable agreement (given uncertainties) with the fading-corrected pIRIR$_{225}$ ages and the pIRIR$_{290}$ ages. The pIt-IR data thus provide some additional support for the antiquity of the Cady Mountain deposits, with the benefit of being obtained independently of the harder to bleach (slowest fading)

pIRIR$_{290}$ signal. The tendency to be slightly older than the pIRIR$_{290}$ signal could suggest some fading effects of the pIRIR$_{290}$ signal (mean g-value$_{2days}$ 1.7 ± 0.3 %; Table S4), but this would require further investigation (and the ages do overlap when the 2 sigma uncertainties are considered).

Overall, these results suggest the pIRIR$_{225}$ is affected by anomalous fading, but for many of the analysed samples (excepting those already showing clear stratigraphic age inversions) the various post-IR signals, each with differing bleaching properties, compare reasonably well, suggesting that for most samples the pIRIR$_{290}$, the fading-corrected pIRIR$_{225}$ or the pIt-IR ages are reasonable burial age estimates. However, the data in Fig. 8 exclude three samples for which substantial age inversions were already apparent (i.e. upper CN section). These results are an obvious cause of concern in terms of incomplete bleaching and as such, a suite of single grain analyses were undertaken, using samples initially interpreted as completely and potentially incompletely bleached.

4.3. Single grain pIRIR

Single grain measurements were undertaken by mounting individual K-feldspar grains onto the centre of stainless-steel disks using silkospray (a single grain IR laser system was not available at the time of analysis). This approach previously produced ages in good agreement with independent dating at Harper and Silver Lake (Carr et al., 2019). For D$_e$ measurement, we employed the same pIRIR$_{225}$ protocol utilised for the multi-grain analyses. After measurement the disks were re-inspected under white light to ensure only disks hosting a single grain were analysed. The distributions of individual grain sensitivities (response of each measured grain to the administered test dose T$_n$; i.e. counts sec^{-1} Gy^{-1}), mirror previous observations (Trauerstein et al., 2012; Rhodes, 2015; Smedley et al., 2019) in that the signal yield from K-feldspars grains is substantially higher than is typical for quartz. In this instance ~50 % of the pIRIR$_{225}$ signal is produced by 15–20 % of the grains. Thus, on a 2 mm aliquot of ~100 grains it is likely >10 grains contribute significantly to the IRSL signal, and that there is significant signal averaging.

Single grain analyses of sample PK14–1-4 provided a useful benchmark; for the single aliquot measurements this site produced stratigraphically concordant ages (Table 1) with good agreement between ages derived from signals with different bleaching characteristics (i.e. fading-corrected pIRIR$_{225}$ and pIRIR$_{290}$, and quartz; Table 1). It is perhaps telling that this locale lacks the immediately adjacent rock slopes of other sites and that it is dominated by medium grained, well-sorted aeolian sands (Fig. S1d). The single grain measurements produced a fading corrected pIRIR$_{225}$ age of 36 ± 3 ka, compared to the single aliquot age of 39 ± 3 ka. The data also imply – as observed by Carr et al. (2019) for the Harper and Silver Lake shoreline deposits – that reasonably well bleached K-feldspar grains may produce OD values of 30–40 %.

Considering the more problematic CN upper section, the single grain equivalent doses (CN13-1-2, CN13-2-1, CN13-3-1) all deviated significantly from their multi-grain estimates (Table 2) and exhibited considerable overdispersion (OD = 87–106 % Table 2). However, in each case there is a cluster of lower D$_e$ grains (~30 Gy), accompanied by grains with several hundred Gy equivalent doses (Fig. 9). These data suggest the multi-grain feldspar measurements were affected by incomplete bleaching, and that their broad (rather than skewed) single aliquot D$_e$ distributions (Fig. S7) reflect the inclusion of multiple incompletely bleached grains in most aliquots. These low D$_e$ single grain populations were not specifically associated with insensitive grains (colour coding Fig. 9 and Fig. S8), and there is equivocal evidence for a "declining baseline" effect (i.e. systematically lower post-IR D$_e$s for less sensitive grains; Rhodes, 2015). To estimate ages for these samples, we applied a finite mixture model (FMM) to the data (Galbraith and Green, 1990). This was run for a range of populations (k) and with the intrinsic OD

Table 2

Single grain IRSL and pIRIR$_{225}$ measurement results. Grains were initially accepted if: 1) their test dose error was <20 %, and 2) T_n was >3 sigma above background. Grains were then rejected (indicated in the "n/N" columns) if: 3) the saturating exponential dose-response curve could not be reliably fitted (interpolated) to the measured L_x/T_x ratios; 4) recycling ratios were outside 2 sigma uncertainties of unity; 5) recuperation was >5 % of L_n/T_n. Fading correction following Huntley and Lamothe (2001) was applied using the site average g-values$_{2days}$ obtained in the single aliquot analysis.

Sample	Total measured	IR 50 n/N	IR50 CAM D_e (Gy)	IR50 OD (%)	pIRIR$_{225}$ n/N	pIRIR$_{225}$ CAM D_e (Gy)	pIRIR$_{225}$ OD (%)	pIRIR$_{225}$ FMM components	Method	IR50 age (ka) (Fading corrected in parentheses)	pIRIR$_{225}$ age (ka) (Fading corrected in parentheses)
Cady North (Slope-Valley fill composite)											
CN13-1-2	192	52/78	21.7 ± 2.8*	85 ± 9	64/81	53 ± 7	106 ± 10	**24 ± 2 (61 %)** 141 ± 23 (29 %) 320 ± 95 (10 %)	FMM	2.9 ± 0.3 **(7.1 ± 1.9)**	5.4 ± 0.5 **(6.8 ± 0.6)**
CN13-2-1	96	35/41	27.0 ± 4.0*	80 ± 10	37/40	58 ± 10	99 ± 12	**29 ± 2 (63 %)** 135 ± 16 (25 %) 347 ± 66 (11 %)	FMM	4.0 ± 0.4 **(10 ± 3)**	6.4 ± 0.5 **(8.0 ± 0.7)**
CN13-3-1	96	41/50	42.2 ± 6.9*	99 ± 11	44/52	81 ± 11	87 ± 9	**31 ± 2 (40 %)** 105 ± 6 (36 %) 245 ± 20 (24 %)	FMM	5.0 ± 0.9 **(12 ± 4)**	6.9 ± 0.5 **(8.7 ± 0.7)**
CN13-4-1	192	55/61	15.3 ± 1.1*	44 ± 5	56/61	31 ± 2*	35 ± 4	n/a	CAM	3.5 ± 0.3 **(8.7 ± 2.2)**	6.8 ± 0.5 **(8.5 ± 0.7)**
CN13-5-1	133	43/55	100 ± 8*	50 ± 6	44/46	222 ± 15*	34 ± 4	n/a	CAM	24 ± 2	52 ± 4 **(68 ± 6)**
Soldier Mountain (Sand ramp)											
SM13-1-1	68	59/62	75 ± 6*	51 ± 5	52/60	171 ± 11*	41 ± 4	n/a	CAM	18 ± 2	40 ± 3 **(53 ± 5)**
SM13-3-1	66	54/65	87 ± 6*	40 ± 4	57/60	192 ± 10*	29 ± 3	n/a	CAM	20 ± 2	44 ± 3 **(58 ± 5)**
Cady Peak (PK Sand ramp)											
PK14-1-4	57	36/44	66 ± 8*	67 ± 8	32/35	132 ± 11	39 ± 5	n/a	CAM	14 ± 2	29 ± 2 **(36 ± 3)**

* Outlier removed prior to averaging using nMAD – see radial plot for illustration.

values (sigma) (e.g. Galbraith and Roberts, 2012). The log-likelihood and Bayes Information Criterion tended to maximise/minimise (respectively) for sigma values of 30–35 %, consistent with the natural (assumed well-bleached) OD values obtained at Harper and Silver Lake and (likely well-bleached) Cady Peak (PK). In each case the aforementioned ~30 Gy D_e cluster comprised 40–63 % of the grains. The resulting ages span 5.4 ± 0.5 to 6.9 ± 0.5 ka (6.8 ± 0.6 to 8.7 ± 0.7 ka with fading correction; Huntley and Lamothe, 2001), and are stratigraphically concordant.

By contrast, two samples lower down the CN section produced single grain results that are less dispersed and closer to the multi-grain aliquot results. For CN13-4-1 a single grain D_e of 31 ± 2 Gy was obtained (single aliquot D_e 45 ± 2 Gy) with the OD (47 % for all grains, 35 ± 4 % with outliers removed) much reduced compared to the overlying samples (Fig. 9). The sample (CN13-5-1) immediately below the site's prominent palaeosol (Fig. S1g), exhibited low OD for both the multi-grain (2 ± 2 %) and single grain data (OD 49 ± 6 % for all grains, 34 ± 4 % with outliers removed) and the single grain pIRIR$_{225}$ age (52 ± 4 ka) was indistinguishable from the multi-grain age (55 ± 3 ka; Tables 1 and 2). For the upper CN section, we thus infer a mixture of well-bleached (largely aeolian) grains and one or more population(s) of partially bleached (slope/fluvially-transported) grains. The FMM outputs imply as many as half of the grains may be incompletely bleached in parts of the upper section above the palaeosol. The fact this is not always the case (CN13-4-1), implies differences between individual beds/depositional events.

For Soldier Mountain, the single grain data for sample SM13-1-1 from the uppermost unit V were moderately overdispersed (45 % for all grains, 41 ± 4 % with outliers removed) and the single grain pIRIR$_{225}$ CAM D_e (171 ± 11 Gy) was somewhat lower than the multi-grain aliquot pIRIR$_{225}$ CAM D_e (227 ± 8 Gy). However, there was no evidence for any population of grains that would generate ages commensurate with

previous dating at this site (Fig. 9) (Rendell and Sheffer, 1996; Bateman et al., 2012). Similarly, the single grain pIRIR$_{225}$ D_e for the subjacent sample SM13-3-1 (192 ± 10 Gy), was within 2 sigma uncertainties of the SM13-1-1 D_e and produced a stratigraphically concordant age. Inter-grain scatter (OD = 37 ± 4 % for all grains) was lower and more comparable to the assumed well-bleached Cady Peak (PK) site. The greater scatter observed for SM13-1-1 is perhaps surprising given the unambiguously aeolian nature of unit V (Fig. S1; Bateman et al., 2012). This unit is however characterised by abundant rhizoliths, which might imply some post-depositional mixing. Given that variability in single grain K content and fading rates are yet to be explored, and the number of analysed grains is relatively low, it is difficult to evaluate this further. Regardless, the single grain results suggest the Soldier Mountain sand ramp is very unlikely to be younger than 40 ka, supporting the "long chronology" implied by the initial single aliquot data. Geomorphic observations that speak to this issue are discussed below.

5. Discussion

5.1. Evaluation of luminescence dating protocols for the Mojave

These results suggest a need to re-evaluate elements of our understanding of the Mojave landscape history, particularly interpretations currently hinging on luminescence chronologies. We infer: 1) luminescence ages based on low temperature IRSL measurements are significantly and consistently impacted by anomalous fading (e.g. Table 1); 2) Mojave quartz properties vary greatly, but are often unsuitable; 3) post-IR IRSL approaches have potential to mitigate the issue of fading, and can often be sufficiently bleached (even the pIRIR$_{290}$ signal). Notwithstanding, in some contexts, incomplete bleaching of the post-IR signal remains a risk and the pIRIR$_{225}$ is seemingly still affected by some
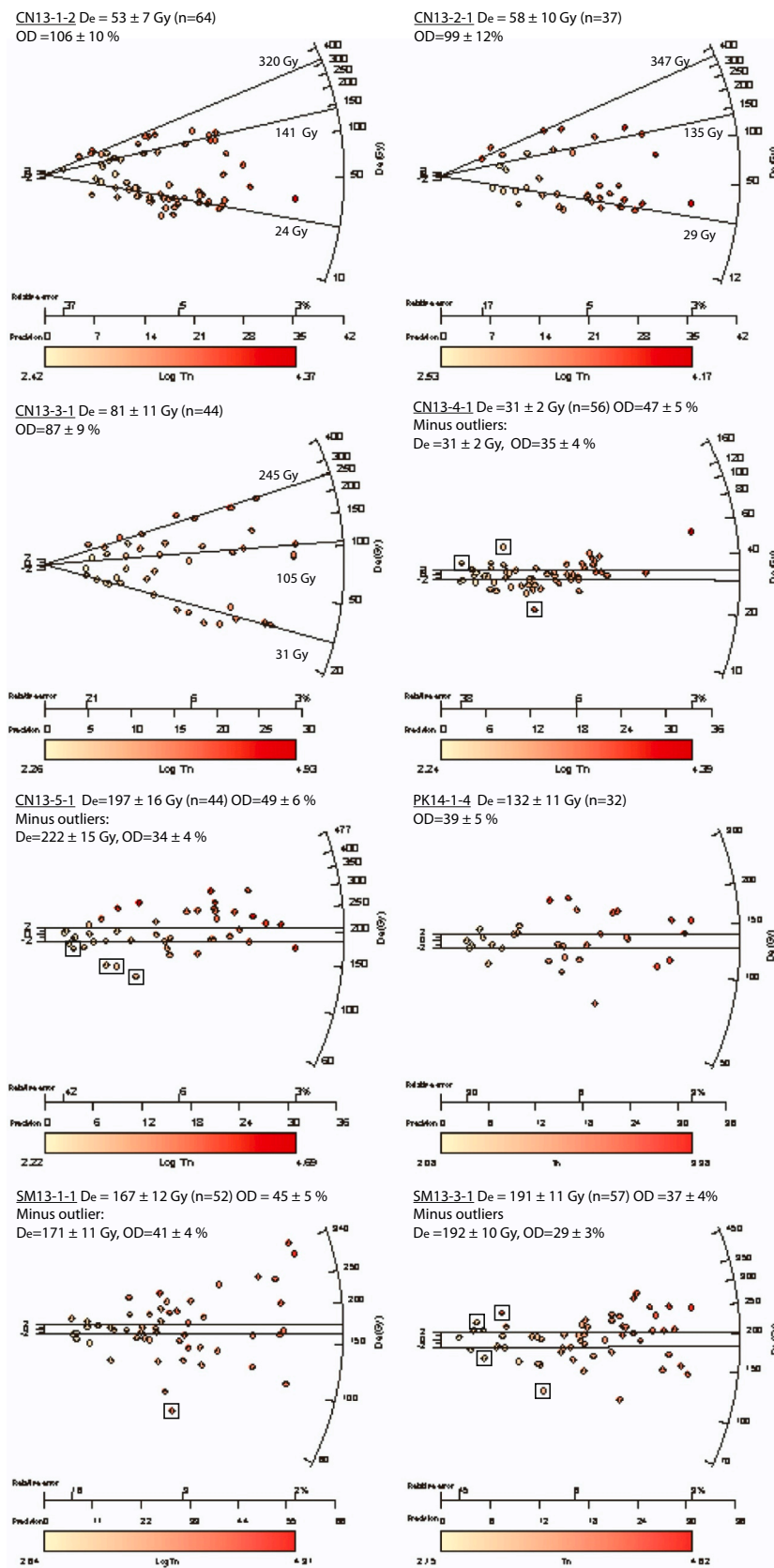
Fig. 9. Single grain radial plots. Each grain is colour coded by log T_n in order to assess the relationship between D_e and sensitivity (Rhodes, 2015). Where applied, the outputs of the finite mixture models are also shown. For samples using CAM D_e estimates, outliers identified using nMAD and excluded before averaging and age calculation (Table 2) are indicated by the square boxes, with the CAM D_e and OD without outlier removal also reported.

fading. Here we consider either the pIRIR$_{290}$ or fading corrected pIRIR$_{225}$ (from single grain analysis where appropriate) results are the most reasonable estimates of site age. These suggest an age range for sand ramps spanning ~118 ka (Middle Cady sand ramp) to ~40 ka (Cady Peak), with sand ramp formation at the western margins of the Cady Mountains largely occurring ~70–80 ka (Soldier Mountain), coeval with accretion of the lower section of the Slope-Valley Composite site at Cady North (~70 ka). Mid-Holocene dune activity occurred as interior sandsheets (DN) and marginal valley-fills (WC), with a phase of early Holocene accretion (interbedded with slope deposits) at the Cady North (CN) composite site.

Considering the mixed performance of quartz, feldspar contamination is a risk for routine preparation methods. The use of post-IR (blue) approaches may not fully address this issue either; for instance, Bateman et al. (2022, their Fig. 8) noted that prior IR stimulation may be insufficient to remove the impact of feldspar contamination on the subsequent quartz OSL measurement in the presence of feldspar inclusions. Additionally, we note instances of a weak fast component, low intrinsic sensitivity and high aliquot rejection rates. These issues potentially manifest in the datasets of some previous studies, where high aliquot rejection rates (using typical quartz SAR criteria; see Table S2) have been reported (e.g. Xie et al., 2019; Sweeney et al., 2020). The Mojave River catchment drains the granitic rocks of the San Bernardino Mountains, ~150 km to the west and the sediment transport rate from the mountain front through the Mojave catchment is quite rapid (McGuire and Rhodes, 2015; Cyr et al., 2015). This short transportation-storage cycle history may be a factor behind the observed insensitivity (e.g. Pietsch et al., 2008) and for sand ramps this may be compounded by any input of "fresh" quartz grains from the bedrock immediately above the ramps.

K-feldspar performs better (Table S3), but bleaches more slowly (McGuire and Rhodes, 2015). Modern dunes within the Mojave River channel show that the pIRIR$_{225}$ and the pIRIR$_{290}$ signals are reduced to low values under ideal (aeolian) conditions (Fig. S5) and at several sites in the Cady Mountains the concordance between the ages derived from different post-IR signals, including the pIt-IR method, suggests bleaching may not always be an issue. However, in some piedmont landforms (the Slope-Valley Composite) incompletely bleached grains are present and are presumably derived from adjacent slopes. The single grain data from the CN section support this notion, with both the IR$_{50}$ and pIRIR$_{225}$ signals generating multi-modal single grain D$_e$ distributions, and the high equivalent doses of some grains consistent with short transport distances and high pre-existing (geological) palaeodoses. The typical distribution of single grain IRSL sensitivities means there is a high probability that most 2 mm multi-grain aliquots will include unbleached grains, producing broad, but un-skewed, single aliquot equivalent dose distributions (Fig. S7). However, the data available thus far suggest incomplete bleaching mostly affects Holocene-aged samples (Fig. 6; cf Fig. 8). Additionally, it is most apparent at sites associated with a visibly-significant gravel (non-aeolian) component (DN, upper CN; Fig. S1g), and sites comprising well-sorted, sand-rich sediment with distant slope (i.e. non-aeolian) sediment sources (i.e. Middle Cady (MC) and Cady Peak (PK) sand ramps, and the Western Cady (WC) Valley fill), are generally associated with low OD and stratigraphically concordant ages (Figs. 7, S1d and S1e; Table 1 and S5).

5.2. The age of the Soldier Mountain sand ramp

The single aliquot pIRIR and pIT-IR ages suggest the Soldier Mountain sand ramp ceased to accumulate at ~70–80 ka (Table 1), rather than 8–11 ka (Bateman et al., 2012). Does the geomorphic context support an older chronology? Given predicted and measured (over three years) rates of downslope (coarse) sediment transfer, Bateman et al. (2012) noted that their quartz OSL age range was extremely difficult to reconcile with the incorporation of stone lines and talus deposits within the ramp itself, and then surface desert pavement (Fig. 10) development


Fig. 10. A) Looking south across the lower slopes of the Soldier Mountain sand ramp. Apparent is the break of slope (and a significant change in surficial materials) at ~543 m asl, the approximate altitude of the late Pleistocene maximum high stand of Lake Manix; **B**) soil development in the uppermost sediments as exposed at the Soldier Mountain quarry; note the loss of original bedding structure and rubification of this layer; **C**) Stone pavement and desert varnish development on the surface of the Soldier Mountain sand ramp (lower surface on left-hand side of the upturned clast).

in the last ~8 ka (i.e. youngest OSL age to the present). The new pIRIR ages provide a much longer time window to emplace the internal (e.g. unit III) stone lines (up to ~30 ka) (Table 1), and imply prolonged stability of the upper surface. Bateman et al. (2012) proposed fluvio-aeolian creep as a plausible mechanism for moving stones down the sandy ramp surface, arguing this could move stones downslope faster than has been measured for rocky slopes in the Mojave. This was necessary to account for the rapidity of emplacement implied by their quartz OSL chronology. While the basic mechanism may well be correct, the longer chronology presented here removes the need to infer the most extreme values for variables such as slope within such sediment transport rate calculations (ibid).

It is also notable that the sand ramp exhibits a pronounced break of slope at 543 m asl (Fig. 10a), which corresponds closely to the maximum heights attained by Lake Manix on several occasions between 40 and 25 ka (Reheis and Redwine, 2008; Reheis et al., 2015). Indeed, Lancaster and Tchakerian (1996; p163) specifically ascribed this slope break to the "highest" Lake Manix shoreline. This would imply the lower slopes of Soldier Mountain sand ramp were emplaced prior to ~40 ka. A slower accumulation rate and longer surface stability is also compatible with the extensive formation of rhizocretions and pedogenic carbonates within unit V (e.g. Harden et al., 1991), and the ramp's rubified upper surface sediments (Fig. 10b). The latter are akin to the palaeosol observed at CN (which itself outcrops at several locations on the north Cady Mountain flank).

5.3. Implied timings of topographic dune formation in the Cady Mountains

The site ages are arranged by accommodation space type in Fig. 11, with the resulting age distribution suggesting potential for aeolian sediment accumulation throughout much of the last glacial cycle,
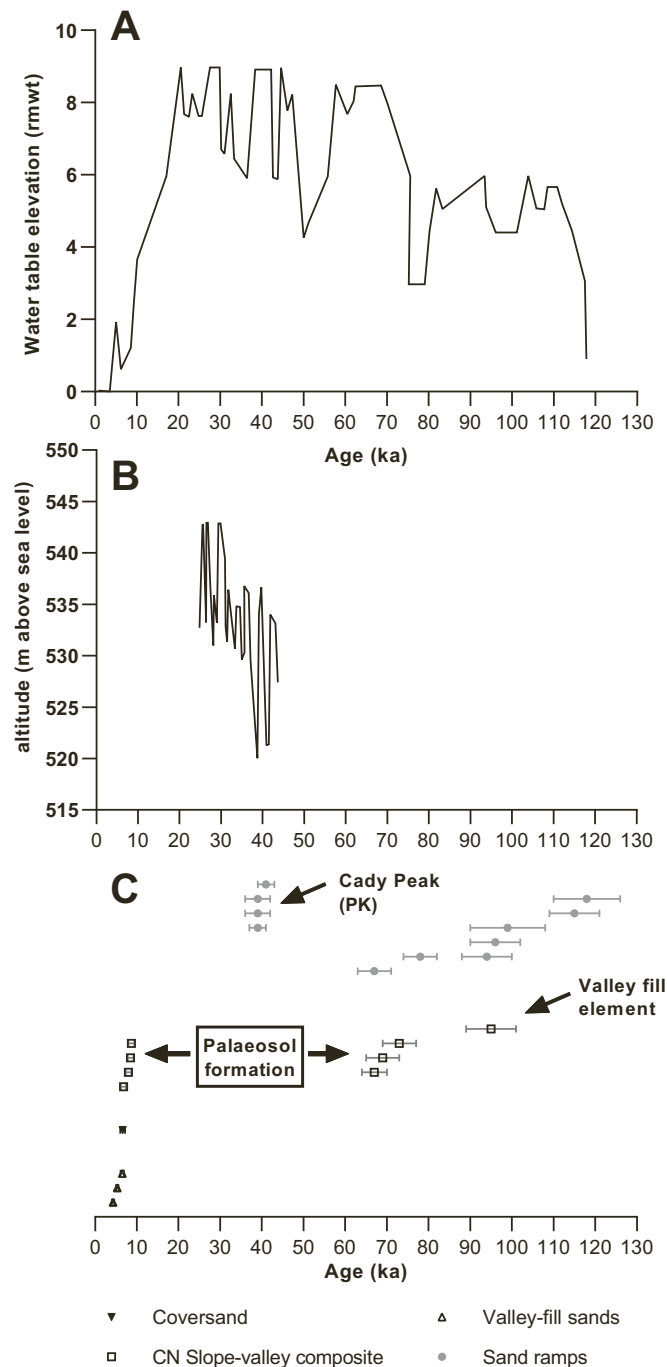
Fig. 11. A: Proxy of regional moisture availability as obtained from the Devil's Hole water table reconstruction (Wendt et al., 2018) (rmwt = relative to modern water table); **B**: Lake Manix lake level record for MIS 3 and 2 (Reheis et al., 2015). **C**: Summarised Cady Mountain luminescence ages organised by accommodation space type (following Hay et al., 2021). The ages comprise the single aliquot pIRIR$_{290}$ or fading-corrected single aliquot pIRIR$_{225}$ ages, except for the upper section of CN Slope-Valley Composite site, where the fading-corrected single grain pIRIR$_{225}$ FMM output is plotted (Table 2). Only the fading-corrected pIRIR$_{225}$ basal age for the DN coversands (DN14-1-1) is shown as an estimate of the approximate site age.

excepting ~40–9 ka. Considering the ages by topographic context, there are hints the record is context dependent (e.g. Hay et al., 2021). Notably, the oldest ages are associated with sand ramps, while the youngest ages are associated with sandsheets and valley-fill deposits. While the new ages imply much greater antiquities than commonly assumed for Mojave sand ramps (cf. Fig. 2), they are consistent with previous arguments that sand ramps can operate as long-term sediment stores (Bertram, 2003; Rowell et al., 2018a, b). The prolonged presence of sand ramps on the margins and within the interior of the Cady Mountains (SM, RD, MC, PK) implies long-term potential to store sediment and – due to filling of windward (i.e. western flank) accommodation spaces – to facilitate the delivery of sands downwind, into the interior of the mountain block. The latter is required for the formation of the downwind sandsheet at DN, which most-likely incorporated aeolian sands during the Holocene (basal age; Fig. 11) (Hay et al., 2021). The upper sediments of the Middle Cady (MC) sand ramp, just 4 km to the south, are ~100,000 years older, implying long-term supply (and storage) of aeolian sediment in the central Cady Mountains and significant spatial complexity in the patterns of deposition / preservation within this complex mountain block topography (Hay et al., 2021).

5.4. Palaeoenvironmental context for regional aeolian activity

Lake Manix and/or the Mojave River have been proposed as key sediment sources for aeolian landforms in this region (Kocurek and Lancaster, 1999; Bateman et al., 2012). Lake Manix intermittently existed adjacent to the Cady Mountains throughout the middle to late Pleistocene (Reheis et al., 2012; Fig. 1). The most detailed evidence (based on radiocarbon dating) for the lake's status exists for MIS 3 onwards, with several high-stands ~43 to 26 ka, and drainage ~25 ka with the Afton Canyon overtopping (Meek, 1999, 2004; Reheis et al., 2015). The Mojave River however continued to intermittently sustain Coyote Lake and potentially Troy Lake, which is immediately upwind of the Cady Mountain western flank area, into late MIS 2 (Meek, 2004; Miller et al., 2019).

An early Holocene age for Soldier Mountain (Bateman et al., 2012) was proposed to be compatible with a scenario of Late Pleistocene Lake Manix drainage (sediment source) followed by early Holocene aridification (sediment availability). The new ages do suggest early to mid-Holocene aeolian sediment accumulation (see also Laity, 1992), but focused elsewhere; Valley-Fill at WC and the upper parts of the Slope-Valley Composite CN section on the northern margin of the Cady Mountains. Indeed, all of the *sand ramps* identified so far are seemingly older than MIS 3. What prompted their formation is thus much less clear; certainly, the positions / states of the Mojave River and Lake Manix during MIS 3 - MIS 5 are weakly defined. Jefferson (2003) noted that of the Manix Formation deposits in the Manix Basin area, the older ages from Member D date to between 48 and 68 ka, implying some MIS 4 inundation (and thus varied sediment delivery during such times), but presently there is insufficient information to infer connections to the Cady Mountain sand ramps. Notwithstanding, the most obvious "gap" in age across all accommodation space types is the period ~40 ka to the early Holocene (Fig. 11), which is coincident with the most humid period of the late Pleistocene (MIS 3-2; Pigati et al., 2011; Wendt et al., 2018; Fig. 11). Soil development is apparent at this time, evidenced by the palaeosol at CN; sediment availability and aeolian sediment transport were seemingly suppressed during this period.

Regardless of timing, it is likely that sand ramps and topographic dunes across this region formed during "windows of opportunity", where sediment supply and availability requirements were met, at least locally, if not regionally (Tchakerian and Lancaster, 2002). Bateman et al. (2012) proposed such a window in the early Holocene for Soldier Mountain, but the new ages imply such windows (also?) existed in MIS 3 - MIS 5. Site location, topographic context and historical contingency likely operated to determine how individual accommodation spaces were filled, emptied and refilled with sand (compare the MIS 5 age

Middle Cady Sand Ramp with the nearby Holocene Valley fill site (WC)), and also whether some piedmont surfaces (i.e. sand ramps) acted as sediment traps (building a sand ramp) or zones of transfer (i.e. a pre-existing sand ramp facilitates transport beyond the mountain front into the Cady Mountain interior). It is noteworthy that no individual locale or topographic context in the Cady Mountains preserves a record of aeolian sedimentation spanning the full range of ages identified.

Finally, this study shows the value of revisiting chronological datasets as methods mature. As works on databases containing luminescence data – such as the INQUA Dunes Atlas (Lancaster et al., 2016) and the BRITICE Chrono database (Small et al., 2017) – have also argued, it is important to evaluate the reliability of historical laboratory analyses. For luminescence dating, key criteria most obviously pertain to the equivalent dose measurement protocol and developments therein (multi vs single aliquot luminescence methods). In this sense, a large proportion of published ages in Mojave region do not meet the "Green" quality control standards proposed by Small et al. (2017) and applying these criteria greatly reduces the number of acceptable ages that can be included in a regional synthesis, as does the less stringent criterion (Fig. 12) of only confirmed use of the SAR protocol. Indeed, as Soldier Mountain has demonstrated, the SAR protocol alone is no guarantee of reliability and the need to report all quality control metrics – particularly in regions that are not well studied, or in which problematic phenomena have been reported – is illustrated. Fortunately, here we were able to access the original materials used in one published work,

allowing us to explain some age discrepancies. It is also worth noting that in the case of Soldier Mountain, Bateman et al. (2012) explicitly recognised that the luminescence ages obtained were very difficult to reconcile with understandings of contemporary geomorphic processes. However, it is often the ages alone that are cited or imported into databases; a salient reminder that (geomorphic) context matters when interpreting and synthesising luminescence ages. Given this, and the unexpectedly old ages generated in the present study, there is value in revisiting the history of aeolian activity in this region; the results imply a far deeper history than previously assumed that, with due awareness of the issue of bleaching, can potentially be probed with the post-IR IRSL approach.

6. Conclusions

The Mojave River catchment contains an array of aeolian landforms, particularly topographically-controlled dunes and sand ramps, which have been considered indicative of, and instructive in understanding, long-term landscape responses to climatic and hydrological change. A critical review of existing chronologies for topographic dune and sand ramp formation, in conjunction with our new results, suggests a need to reconsider the timings of these responses. We show that that low temperature IRSL signals consistently suffer high rates of anomalous fading, and that quartz OSL requires rigorous scrutiny to obviate, or at least identify, the combined problems of K-feldspar contamination and a

All contexts
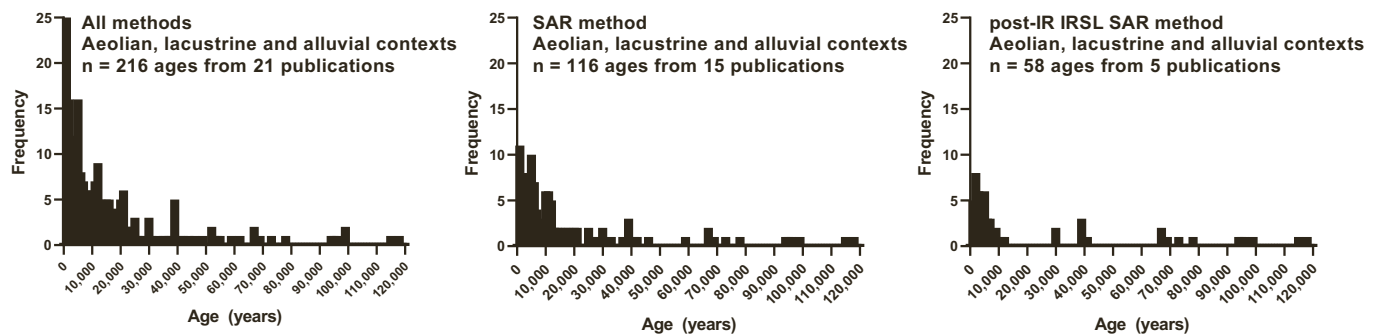
Aeolian landforms
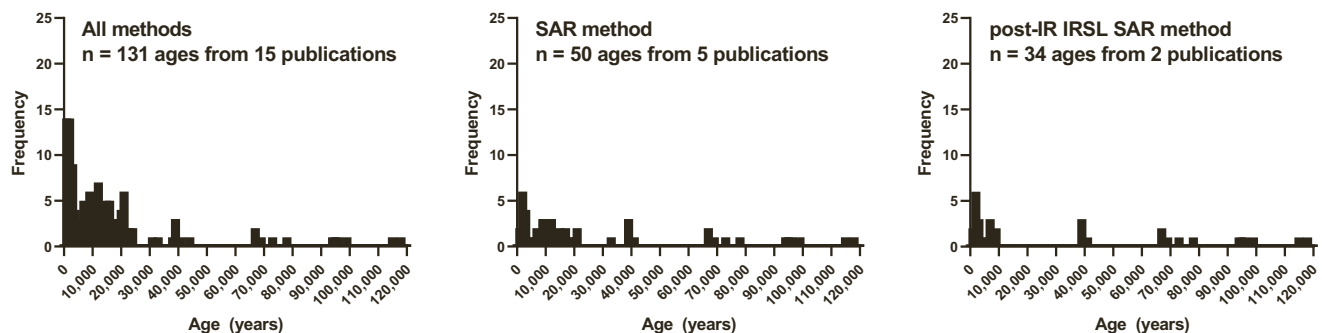
Fig. 12. Luminescence age compilation for the Mojave Desert region. These histograms compile the present study's data with published ages (1994 to 2022) across the study region in Fig. 1 and somewhat beyond (as far north as Death Valley (Sohn et al., 2007) and as far south as Big Marias, 10 km west of the Colorado River (Rendell and Sheffer, 1996)). Where multiple minerals/methods were used to produce ages for a single sample, the K-Feldspar IRSL results were plotted. The purpose here is to show the broad range in apparent ages and the impact on the dataset size of selecting only SAR-derived ages as a quality-control filter, and then only post-IR IRSL feldspar methods as a further filter – no palaeoenvironmental significance is implied/inferred. Note that for ease of plotting several substantially older ages from lacustrine settings (Mahan et al., 2007; Reheis et al., 2020) were excluded from the histograms. The list of works used in the compilation is noted in Table S8.

weak quartz fast component. As a result, we propose that many previous luminescence-based chronologies for the Mojave are of questionable reliability.

Considering the topographic dunes and sand ramps in the Cady Mountains – a location adjacent to and downwind of the Mojave River and palaeolake Manix – while the issue of incomplete bleaching remains, particularly for younger sites with a proximal slope sediment source, the post-IR IRSL results presented here suggest: 1) an age range of >100,000 years across a suite of aeolian sediments; 2) that sand ramps may be long-lived landscape elements, and significantly older than earlier works inferred; 3) there may be temporal patterns in the timing of sand accumulation across different topographic settings (accommodation space types) e.g. the relatively young aeolian deposits in the Cady Mountains are primarily associated with sandsheet and valley fill accommodation space types. Disentangling the roles of climatic change and topography in controlling the trapping and preservation of aeolian sediments in the topographically complex Cady Mountains, or indeed the wider Mojave Desert requires a far more extensive sample set, but the data available at present suggest potential to refine this story. An evaluation of the published luminescence dating from this region suggests many published ages do not meet typically accepted reliability criteria (in general and specifically in relation to the present findings). On this basis, the regional aeolian geomorphic history can be considered weakly constrained at present, with further implications for our models of aeolian system response and regional paleoenvironmental interpretations.

CRediT authorship contribution statement

Andrew S. Carr: Writing – original draft, Supervision, Resources, Methodology, Investigation, Formal analysis, Data curation, Conceptualization. **Alex S. Hay:** Writing – review & editing, Investigation. **Mark D. Bateman:** Writing – review & editing, Resources, Investigation. **Ian Livingstone:** Writing – review & editing, Supervision, Investigation, Conceptualization. **D. Mark Powell:** Writing – review & editing, Supervision, Investigation, Conceptualization.

Declaration of competing interest

The authors declare the following financial interests/personal relationships which may be considered as potential competing interests: Alex S Hay reports financial support was provided by Natural Environment Research Council. If there are other authors, they declare that they have no known competing financial interests or personal relationships that could have appeared to influence the work reported in this paper.

Data availability

Data will be made available on request.

Appendix A. Supplementary data

Supplementary data to this article can be found online at https://doi.org/10.1016/j.geomorph.2024.109349.

References

Aitken, M.J., 1985. Thermoluminescence Dating. Academic Press, London and New York.

Auclair, M., Lamothe, M., Huot, S., 2003. Measurement of anomalous fading for feldspar IRSL using SAR. Radiat. Meas. 37, 487–492.

Bateman, M.D., Bryant, R.G., Foster, I.D.L., Livingstone, I., Parsons, A.J., 2012. On the formation of sand ramps: a case study from the Mojave Desert. Geomorphology 161–162, 93–109.

Bateman, M.D., Bryant, R.G., Luo, W., 2022. Getting the right age? Testing luminescence dating of both quartz and feldspars against independent age controls. Quat. Geochronol. 72, 101366.

Bell, W.T., 1979. Thermoluminescence dating: radiation dose-rate data. Archaeometry 21, 243–245.

Bertram, S., 2003. Late Quaternary Sand Ramps in South-Western Namibia-Nature, Origin and Palaeoclimatological Significance. Doctoral Thesis,. University of Würzburg: Würzburg, Germany.

Blaney, H.F., 1957. Evaporation study at Silver Lake in the Mojave Desert, California. EOS Trans. Am. Geophys. Union 38, 209–215.

Bøtter-Jensen, L., Mejdahl, V., 1988. Assessment of beta dose-rate using a GM multicounter system. Nucl. Tracks Radiat. Meas. 14, 187–191.

Burow, C., 2024. calc_CosmicDoseRate( ): calculate the cosmic dose rate. Function version 0.5.2. In: Kreutzer, S., Burow, C., Dietze, M., Fuchs, M.C., Schmidt, C., Fischer, M., Friedrich, J., Mercier, N., Philippe, A., Riedesel, S., Autzen, M., Mittelstrass, D., Gray, H.J., Galharret, J. (Eds.), Luminescence: Comprehensive Luminescence Dating Data Analysis. R package Version 0.9.24. https://CRAN.R-project.org/package=Luminescence.

Buylaert, J.-P., Murray, A.S., Thomsen, K.J., Jain, M., 2009. Testing the potential of an elevated temperature IRSL signal from K-feldspar. Radiat. Meas. 44, 560–565.

Buylaert, J.-P., Jain, M., Murray, A.S., Thomsen, K.J., Theil, C., Sohbati, R., 2012. A robust feldspar luminescence dating method for Middle and Late Pleistocene sediments. Boreas 41, 435–451.

Buylaert, J.-P., Murray, A.S., Gebhardt, A.C., Sohbati, R., Ohlendorf, C., Thiel, C., Wastegård, S., Zolitschka, B., 2013. Luminescence dating of the PASADO core 5022-1D from Laguna Potrok Aike (Argentina) using IRSL signals from feldspar. Quat. Sci. Rev. 71, 70–80.

Carr, A.S., Hay, A.S., Powell, D.M., Livingstone, I., 2019. Testing post-IR IRSL luminescence dating methods in the southwest Mojave Desert, California, USA. Quat. Geochronol. 49, 85–91.

Clarke, M.L., 1994. Infra-red stimulated luminescence ages from aeolian sand and alluvial fan deposits from the eastern Mojave Desert, California. Quat. Sci. Rev. 13, 533–538.

Clarke, M.L., Rendell, H.M., 1998. Climate change impacts on sand supply and the formation of desert sand dunes in the south-west U.S.A. J. Arid Environ. 39, 517–531.

Clarke, M.L., Richardson, C.A., Rendell, H.M., 1995. Luminescence dating of Mojave Desert sands. Quat. Sci. Rev. 14, 783–789.

Clarke, M.L., Wintle, A.G., Lancaster, N.J., 1996. Infra-red stimulated luminescence dating of sands from the Cronese Basins, Mojave Desert. Geomorphology 17, 199–205.

Clarkson, C., Jacobs, Z., Marwick, B., Fullagar, R., Wallis, L., Smith, M., Roberts, R.G., Hayes, E., Lowe, K., Carah, X., Florin, S.A., McNeil, J., Cox, D., Arnold, L.J., Hua, Q., Huntley, J., Brand, H.E.A., Manne, T., Fairbairn, A., Pardoe, C., 2017. Human occupation of northern Australia by 65,000 years ago. Nature 547, 306–310.

Colarossi, D., Duller, G.A.T., Roberts, H.M., 2018. Exploring the behaviour of luminescence signals from feldspars: Implications for the single aliquot regenerative dose protocol. Radiat. Meas. 109, 35–44.

Cunningham, A.C., Wallinga, J., 2010. Selection of integration time intervals for quartz OSL decay curves. Quat. Geochronol. 5, 657–666.

Cyr, A.J., Miller, D.M., Mahan, S.A., 2015. Paleodischarge of the Mojave River, southwestern United States, investigated with single-pebble measurements of [10]Be. Geosphere 11k, 1158–1171.

Duller, G.A.T., 2007. Assessing the error on equivalent dose estimates derived from single aliquot regenerative dose measurements. Ancient TL 25, 15–24.

Duller, G.A.T., Augustinus, P.C., 2006. Reassessment of the record of linear dune activity in Tasmania using optical dating. Quat. Sci. Rev. 25, 2608–2618.

Durcan, J.A., Duller, G.A.T., 2011. The fast ratio: a rapid measure for testing the dominance of the fast component in the initial OSL signal from quartz. Radiat. Meas. 46, 1065–1107.

Edwards, S.R., 1993. Luminescence dating of sand from the Kelso Dunes, California. Geol. Soc. Lond. Spec. Publ. 72, 59–68.

Ellwein, A.M., Mahan, S.A., McFadden, L.D., 2011. New optically stimulated luminescence ages provide evidence of MIS3 and MIS2 eolian activity on Black Mesa, northeastern Arizona, USA. Quat. Res. 75, 395–398.

Enzel, Y., 1992. Flood frequency of the Mojave River and the formation of late Holocene playa lakes, southern California, USA. The Holocene 2, 11–18.

Enzel, Y., Wells, S.G., 1997. Extracting Holocene paleohydrology and paleoclimatology information from modern extreme flood events: an example from southern California. Geomorphology 19, 203–226.

Enzel, Y., Wells, S.G., Lancaster, N., 2003. Late Pleistocene lakes along the Mojave River, southeast California. Special papers - Geological Society of America 61–78.

Evans, J.R., 1962. Falling and climbing sand dunes in the Cronese ("Cat") Mountain Area, San Bernardino County, California. J. Geol. 70, 107–113.

Fuchs, M., Dietze, M., Al-Qudah, K., Lomax, J., 2015. Dating desert pavements – first results from a challenging environmental archive. Quat. Geochronol. 30, 342–349.

Galbraith, R.F., 2003. A simple homogeneity test for estimates of dose obtained using OSL. Ancient TL 21, 75–77.

Galbraith, R.F., Green, P.F., 1990. Estimating the component ages in a finite mixture. International Journal of Radiation applications and Instrumentation. Part D. Nuclear Tracks and Radiation Measurements 17, 197–206.

Galbraith, R.F., Roberts, R.G., 2012. Statistical aspects of equivalent dose and error calculation and display in OSL dating: an overview and some recommendations. Quat. Geochronol. 11, 1–27.

Galbraith, R.F., Roberts, R.G., Laslett, G.M., Yoshida, H., Olley, J.M., 1999. Optical dating of single and multiple grains of quartz from Jinmium rock shelter, northern Australia, part 1, Experimental design and statistical models. Archaeometry 41, 339–364.

Garcia, A.L., Knott, J.R., Mahan, S.A., Bright, J., 2014. Geochronology and paleoenvironment of pluvial Harper Lake, Mojave Desert, California, USA. Quat. Res. 81, 305–317.

Harden, J.W., McFadden, L.D., Hill, C., Mark, R.K., Reheis, M.C., Sowers, J.M., Taylor, E. M., Wells, S.G., 1991. A comparison of four soil chronosequences in the southern Great Basin: rates of soil development and implications for soil chronology. Quat. Res. 35, 383–399.

Hay, A.S., Powell, D.M., Carr, A.S., Livingstone, I., 2021. Characterisation of aeolian sediment accumulation and preservation across complex topography. Geomorphology 383, 107704.

Honke, J.S., Pigati, J.S., Wilson, J., Bright, J., Goldstein, H.L., Skipp, G.L., Reheis, M.C., Havens, J.C., 2019. Late Quaternary paleohydrology of desert wetlands and pluvial lakes in the Soda Lake basin, Central Mojave Desert, California (USA). Quat. Sci. Rev. 216, 89–106.

Huntley, D.J., Baril, M.R., 1997. The K content of the K-feldspars being measured in optical dating or in thermoluminescence dating. Ancient TL 15, 11–13.

Huntley, D.J., Hancock, R.G.V., 2001. The Rb contents of the K-feldspar grains being measured in optical dating. Ancient TL 19, 43–46.

Huntley, D.J., Lamothe, M., 2001. The ubiquity of anomalous fading in K-feldspars and the measurement and correction for it in optical dating. Can. J. Earth Sci. 38, 1093–1106.

Huntley, D.J., Lian, O.B., 2006. Some observations on tunnelling of trapped electrons in feldspars and their implications for optical dating. Quat. Sci. Rev. 25, 2503–2512.

Jacobs, Z., Roberts, R.G., 2015. An improved single grain OSL chronology for the sedimentary deposits from Diepkloof rockshelter, Western Cape, South Africa. J. Archaeol. Sci. 63, 175–192.

Jefferson, G.T., 2003. Stratigraphy and palaeontology of the middle and late Pleistocene Manix Formation, and paleoenvironments of the central Mojave River, southern California. Geol. Soc. Am. Spec. Pap. 368, 43–60.

Kirby, M.E., Knell, E.J., Anderson, W.T., Lachniet, M.S., Palermo, J., Eeg, H., Lucero, R., Murrieta, R., Arevalo, A., Silveira, E., Hiner, C.A., 2015. Evidence for insolation and Pacific forcing of late glacial through Holocene climate in the Central Mojave Desert (Silver Lake, CA). Quat. Res. 84, 174–186.

Kocurek, G., Lancaster, N., 1999. Aeolian system sediment state: theory and Mojave Desert Kelso dune field example. Sedimentology 46, 505–515.

Kreutzer, S., 2024. calc_FadingCorr( ): fading correction after Huntley & Lamothe (2001). Function version 0.4.3. In: Kreutzer, S., Burow, C., Dietze, M., Fuchs, M.C., Schmidt, C., Fischer, M., Friedrich, J., Mercier, N., Philippe, A., Riedesel, S., Autzen, M., Mittelstrass, D., Gray, H.J., Galharret, J. (Eds.), Luminescence: Comprehensive Luminescence Dating Data Analysis. R Package Version 0.9.24. https ://CRAN.R-project.org/package=Luminescence.

Kreutzer, S., Burow, C., Dietze, M., Fuchs, M., Schmidt, C., Fischer, M., Friedrich, J., Mercier, N., Philippe, A., Riedesel, S., Autzen, M., Mittelstrass, D., Gray, H., Galharret, J., 2024. Luminescence: Comprehensive Luminescence Dating Data Analysis. R Package Version 0.9.24. https://CRAN.R-project.org/package=Luminescence.

Kumar, A., Srivastava, P., Meena, N.K., 2017. Late Pleistocene aeolian activity in the cold desert of Ladakh: a record from sand ramps. Quat. Int. 443, 13–28.

Laity, J.E., 1992. Ventifact evidence for Holocene wind patterns in the east-central Mojave Desert. Z. Geomorphol. 84, 73–88.

Lamothe, M., Brisson, L.F., Hardy, F., 2020. Circumvention of anomalous fading in feldspar luminescence dating using Post-Isothermal IRSL. Quat. Geochronol. 57, 101062.

Lancaster, N., Tchakerian, V.P., 1996. Geomorphology and sediments of sand ramps in the Mojave Desert. Geomorphology 17, 151–165.

Lancaster, N., Wolfe, S., Thomas, D.S.G., Bristow, C., Bubenzer, O., Burrough, S., Duller, G.A.T., Halfen, A., Hesse, P., Roskin, J., Singhvi, A.K., 2016. The INQUA dunes atlas chronologic database. Quat. Int. 410, 3–10.

Lancaster, N., Bacon, S.N., Bullard, T.F., Neudorf, C.M., Keen-Zebert, A.K., Decker, D.L., Boggs, M.L., 2022. Tectonic, hydrogeologic, and climatic controls on Late Holocene dune formation, China Lake basin, Indian Wells Valley, California, USA. Quat. Res. 106, 11–27.

Lawson, M.J., Roder, B.J., Stang, D.M., Rhodes, E.J., 2012. OSL and IRSL characteristics of quartz and feldspar from southern California, USA. Radiat. Meas. 47, 830–836.

Lawson, M.J., Daniels, J.T., Rhodes, E.J., 2015. Assessing Optically Stimulated Luminescence (OSL) signal contamination within small aliquots and single grain measurements utilizing the composition test. Quat. Int. 362, 34–41.

Li, B., Jacobs, Z., Roberts, R.G., Li, S.-H., 2014. Review and assessment of the potential of post-IR IRSL dating methods to circumvent the problem of anomalous fading in feldspar luminescence. Geochronometria 41, 178–201.

Livingstone, I., Warren, A. (Eds.), 2019. Aeolian Geomorphology: A New Introduction. John Wiley, Chichester, Sussex.

Mahan, S.A., Miller, D.M., Menges, C.M., Yount, J.C., 2007. Late Quaternary stratigraphy and luminescence geochronology of the northeastern Mojave Desert. Quat. Int. 166, 61–78.

McGuire, C., Rhodes, E.J., 2015. Determining fluvial sediment virtual velocity on the Mojave River using K-feldspar IRSL: initial assessment. Quat. Int. 362, 124–131.

Meek, N., 1989. Geomorphic and hydrologic implications of the rapid incision of Afton Canyon, Mojave Desert, California. Geology 17, 7–10.

Meek, N., 1999. New discoveries about the Late Wisconsinan history of the late Mojave River system. San Bernardino County Museum Association Quarterly 46, 113–117.

Meek, N., 2004. Mojave River history from an upstream perspective. In: Abstracts from the 2004 Desert Symposium, California State University, Desert Studies Consortium. desertsymposium.org.

Mejdahl, V., 1979. Thermoluminescence dating: beta-dose attenuation in quartz grains. Archaeometry 21, 61–72.

Miller, D.M., Dudash, S.L., McGeehin, J.P., 2019. Paleoclimate record for Lake Coyote, California, and the Last Glacial Maximum and deglacial paleohydrology (25 to 14 cal ka) of the Mojave River. In: Starratt, S.W., Rosen, M.R. (Eds.), From Saline to Freshwater: The Diversity of Western Lakes in Space and Time, GSA Special Paper, 536. Geological Society of America.

Muhs, D.R., Reynolds, R.L., Been, J., Skipp, G., 2003. Eolian sand transport pathways in the southwestern United States: importance of the Colorado River and local sources. Quat. Int. 104, 3–18.

Murray, A.S., Olley, J.M., 2002. Precision and accuracy in the optically stimulated luminescence dating of sedimentary quartz: a status review. Geochronometria 21, 1–16.

Murray, A.S., Wintle, A.G., 2000. Luminescence dating of quartz using an improved single-aliquot regenerative-does protocol. Radiat. Meas. 32, 57–73.

Murray, A.S., Wintle, A.G., 2003. The single aliquot regenerative dose protocol: potential for improvements in reliability. Radiat. Meas. 37, 377–381.

Murray, A.S., Thomsen, K.J., Masuda, N., Buylaert, J.P., Jain, M., 2012. Identifying well-bleached quartz using the different bleaching rates of quartz and feldspar signals. Radiat. Meas. 47, 688–695.

Owen, L.A., Bright, J., Finkel, R.C., Jaiswal, M.K., Kaufman, D.S., Mahan, S., Radtke, U., Schneider, J.S., Sharp, W., Singhvi, A.K., Warren, C., 2007. Numerical dating of a Late Quaternary spit-shoreline complex at the northern end of Silver Lake playa, Mojave Desert, California: a comparison of the applicability of radiocarbon, luminescence, terrestrial cosmogenic nuclide, electron spin resonance, U-series and amino acid racemization methods. Quat. Int. 166, 87–110.

Paichoon, M.S., 2020. Analysis of the origin, formation and development of sand ramps on the Eastern slopes of Shirkouh, Yazd, Central Iran. Geomorphology 351, 106891.

Pietsch, T.J., Olley, J.M., Nanson, G.C., 2008. Fluvial transport as a natural luminescence sensitiser of quartz. Quat. Geochronol. 365–376.

Pigati, J.S., Miller, D.M., Bright, J.E., Mahan, S.A., Nekola, J.C., Paces, J.B., 2011. Chronology, sedimentology and microfauna of groundwater discharge deposits in the central Mojave Desert, Valley Wells, California. Geol. Soc. Am. Bull. 123, 185–206.

Prescott, J.R., Hutton, J.T., 1994. Cosmic ray contributions to dose rates for luminescence and ESR dating: large depths and long-term time variations. Radiat. Meas. 23, 497–500.

Reheis, M.C., Redwine, J.L., 2008. Lake Manix shorelines and Afton Canyon terraces: implications for incision of Afton Canyon. In: Late Cenozoic Drainage History of the Southwestern Great Basin and Lower Colorado River Region: Geologic and Biotic Perspectives. Geological Society of America Special Paper, 439, pp. 227–259.

Reheis, M.C., Bright, J., Lund, S.P., Miller, D.M., Skipp, G., Fleck, R.J., 2012. A half-million-year record of paleoclimate from the Lake Manix Core, Mojave Desert, California. Palaeogeogr. Palaeoclimatol. Palaeoecol. 365, 11–37.

Reheis, M.C., Adams, K.D., Oviatt, C.G., Bacon, S.N., 2014. Pluvial lakes in the Great Basin of the western United States—a view from the outcrop. Quat. Sci. Rev. 97, 33–57.

Reheis, M.C., Miller, D.M., McGeehin, J.P., Redwine, J.R., Oviatt, C.G., Bright, J., 2015. Directly dated MIS 3 lake-level record from Lake Manix, Mojave Desert, California, USA. Quat. Res. 83, 187–203.

Reheis, M.C., Caskey, J., Bright, J., Paces, J.B., Mahan, S., Wan, E., 2020. Pleistocene lakes and paleohydrologic environments of the Tecopa basin, California: constraints on the drainage integration of the Amargosa River. Geol. Soc. Am. Bull. 132, 1537–1565.

Reheis, M.C., Miller, D.M., Paces, J.B., Oviatt, C.G., Redwine, J.R., Kaufman, D.S., Bright, J., Wan, E., 2021. Geomorphic history of Lake Manix, Mojave Desert, California: evolution of a complex terminal lake basin. Geomorphology 392, 107901.

Rendell, H.M., Sheffer, N.L., 1996. Luminescence dating of sand ramps in the Eastern Mojave Desert. Geomorphology 17, 187–197.

Rendell, H., Lancaster, N., Tchakerian, V.P., 1994. Luminescence dating of Late Pleistocene aeolian deposits at Dale Lake and Cronese Mountains, Mojave Desert, California. Quat. Sci. Rev. 13, 417–422.

Rhodes, E.J., 2011. Optically stimulated luminescence dating of sediments over the past 200,000 years. Annu. Rev. Earth Planet. Sci. 39, 461–488.

Rhodes, E.J., 2015. Dating sediments using potassium feldspar single-grain IRSL: initial methodological considerations. Quat. Int. 362, 14–22.

Roder, B., Lawson, M., Rhodes, E.J., Dolan, J., McAuliffe, L., McGill, S., 2012. Assessing the potential of luminescence dating for fault slip rate studies on the Garlock fault, Mojave Desert, California, USA. Quat. Geochronol. 10, 285–290.

Rowell, A., Thomas, D.S., Bailey, R.M., Stone, A., Garzanti, E., Padoan, M., 2018a. Controls on sand ramp formation in southern Namibia. Earth Surf. Process. Landf. 43, 150–171.

Rowell, A.L., Thomas, D.S., Bailey, R.M., Holmes, P.J., 2018b. Sand ramps as palaeoenvironmental archives: Integrating general principles and regional contexts through reanalysis of the Klipkraal Sands, South Africa. Geomorphology 311, 103–113.

Schaetzl, R.J., Larson, P.H., Faulkner, D.J., Running, G.L., Jol, H.M., Rittenour, T.M., 2018. Eolian sand and loess deposits indicate west-northwest paleowinds during the Late Pleistocene in western Wisconsin, USA. Quat. Res. 89, 769–785.

Sharp, R.S., 1966. Kelso Dunes, Mojave Desert, California. Geol. Soc. Am. Bull. 77, 1045–1074.

Small, D., Clark, C.D., Chiverrell, R.C., Smedley, R.K., Bateman, M.D., Duller, G.A.T., Ely, J.C., Fabel, D., Medialdea, A., Moreton, S.G., 2017. Devising quality assurance procedures for assessment of legacy geochronological data relating to deglaciation of the last British-Irish Ice Sheet. Earth Sci. Rev. 164, 232–250.

Smedley, R.K., Duller, G.A.T., Roberts, H.M., 2015. Bleaching of the post-IR IRSL signal from individual grains of K-feldspar: Implications for single-grain dating. Radiat. Meas. 79, 33–42.

Smedley, R.K., Buylaert, J.P., Újvári, G., 2019. Comparing the accuracy and precision of luminescence ages for partially-bleached sediments using single grains of K-feldspar and quartz. Quat. Geochronol. 53, 101007.

Smith, R.S.U., 1984. Eolian geomorphology of the Devils Playground, Kelso Dunes and Silurian Valley, California. In: Western Geological Excursions. Vol. 1: Geological Society of America 97th Annual Meeting Field Trip Guidebook, Reno, Nevaday, pp. 239–251.

Sohn, M.F., Mahan, S.A., Knott, J.R., Bowman, D.D., 2007. Luminescence ages for alluvial-fan deposits in Southern Death Valley: Implications for climate-driven sedimentation along a tectonically active mountain front. Quat. Int. 166 (1), 49–60.

Spooner, N.A., 1994. On the optical dating signal from quartz. Radiat. Meas. 23, 563–600.

Steffen, D., Preusser, F., Schlunegger, F., 2009. OSL quartz age underestimation due to unstable signal components. Quat. Geochronol. 4, 353–362.

Sweeney, M.R., McDonald, E.V., Chabela, L.P., Hanson, P.R., 2020. The role of eolian-fluvial interactions and dune dams in landscape change, late Pleistocene–Holocene, Mojave Desert, USA. Geol. Soc. Am. Bull. 132, 2318–2332.

Tchakerian, V.P., Lancaster, N., 2002. Late Quaternary arid/humid cycles in the Mojave Desert and western Great Basin of North America. Quat. Sci. Rev. 21, 799–810.

Thomas, D.S., Bateman, M.D., Mehrshahi, D., O'hara, S.L., 1997. Development and environmental significance of an eolian sand ramp of last-glacial age, Central Iran. Quat. Res. 48, 155–161.

Trauerstein, M., Lowick, S., Preusser, F., Rufer, D., Schlunegger, F., 2012. Exploring fading in single grain feldspar IRSL measurements. Quat. Geochronol. 10, 327–333.

Wendt, K.A., Dublyansky, Y.V., Moseley, G.E., Edwards, R.L., Cheng, H., Spötl, C., 2018. Moisture availability in the southwest United States over the last three glacial-interglacial cycles. Science. Advances 4, eaau1375.

Wintle, A.G., 1973. Anomalous fading of thermo-luminescence in mineral samples. Nature 245, 143–144.

Wintle, A.G., Lancaster, N., Edwards, S.R., 1994. Infrared stimulated luminescence (IRSL) dating of late-Holocene aeolian sands in the Mojave Desert, California, USA. The Holocene 4, 74–78.

Xie, S., Gallant, E., Wetmore, P.H., Figueiredo, P.M., Owen, L.A., Rasmussen, C., Malservisi, R., Dixon, T.H., 2019. A new geological slip rate estimate for the Calico Fault, eastern California: implications for geodetic versus geologic rate estimates in the Eastern California Shear Zone. Int. Geol. Rev. 61, 1613–1641.

Zhang, J., Li, S.-H., 2020. Review of the Post-IR IRSL dating protocols of K-Feldspar. Methods and Protocols 3 (1), 7.

Zimbleman, J.R., Williams, S.H., Tchakerian, V.P., 1995. Sand transport paths. In: Tchakerian, V.P. (Ed.), Desert Aeolian Processes. Chapman & Hall, London.